(12) INTERNATIONAL APPLICATION PUBLISHED UNDER THE PATENT COOPERATION TREATY (PCT)

(19) World Intellectual Property Organization
International Bureau

(43) International Publication Date
15 November 2018 (15.11.2018)

WIPO | PCT

(10) International Publication Number
WO 2018/209104 A1

(51) International Patent Classification:
G02F 1/01 (2006.01) *H01L 51/44* (2006.01)
E06B 9/24 (2006.01) *H01L 51/46* (2006.01)

(21) International Application Number:
PCT/US2018/032088

(22) International Filing Date:
10 May 2018 (10.05.2018)

(25) Filing Language: English

(26) Publication Language: English

(30) Priority Data:
62/504,109 10 May 2017 (10.05.2017) US

(71) Applicant: **ALLIANCE FOR SUSTAINABLE ENERGY, LLC** [US/US]; 15013 Denver West Parkway, Golden, Colorado 80401 (US).

(72) Inventors: **WHEELER, Lance Michael**; 3481 Benton Street, Apartment 1, Wheat Ridge, Colorado 80212 (US). **IHLY, Rachelle Rosemarie**; 2398 Elkhorn Street, Parker, Colorado 80138 (US). **STANTON, Noah James**; 1135 Elizabeth Street, #204, Denver, Colorado 80206 (US). **BLACKBURN, Jeffrey Lee**; 2040 Goldenvue Drive, Golden, Colorado 80401 (US).

(74) Agent: **MCINTYRE, Michael A.**; 15013 Denver West Parkway, Golden, Colorado 80401 (US).

(81) Designated States *(unless otherwise indicated, for every kind of national protection available)*: AE, AG, AL, AM, AO, AT, AU, AZ, BA, BB, BG, BH, BN, BR, BW, BY, BZ, CA, CH, CL, CN, CO, CR, CU, CZ, DE, DJ, DK, DM, DO, DZ, EC, EE, EG, ES, FI, GB, GD, GE, GH, GM, GT, HN, HR, HU, ID, IL, IN, IR, IS, JO, JP, KE, KG, KH, KN, KP, KR, KW, KZ, LA, LC, LK, LR, LS, LU, LY, MA, MD, ME, MG, MK, MN, MW, MX, MY, MZ, NA, NG, NI, NO, NZ, OM, PA, PE, PG, PH, PL, PT, QA, RO, RS, RU, RW, SA, SC, SD, SE, SG, SK, SL, SM, ST, SV, SY, TH, TJ, TM, TN, TR, TT, TZ, UA, UG, US, UZ, VC, VN, ZA, ZM, ZW.

(84) Designated States *(unless otherwise indicated, for every kind of regional protection available)*: ARIPO (BW, GH, GM, KE, LR, LS, MW, MZ, NA, RW, SD, SL, ST, SZ, TZ, UG, ZM, ZW), Eurasian (AM, AZ, BY, KG, KZ, RU, TJ, TM), European (AL, AT, BE, BG, CH, CY, CZ, DE, DK, EE, ES, FI, FR, GB, GR, HR, HU, IE, IS, IT, LT, LU, LV, MC, MK, MT, NL, NO, PL, PT, RO, RS, SE, SI, SK, SM, TR), OAPI (BF, BJ, CF, CG, CI, CM, GA, GN, GQ, GW, KM, ML, MR, NE, SN, TD, TG).

Published:
— *with international search report (Art. 21(3))*

(54) Title: MULTILAYER CARBON NANOTUBE FILM-CONTAINING DEVICES

(57) Abstract: The present disclosure relates to a device that includes an active layer and a first charge transport layer, where the first charge transport layer includes a first layer and a second layer, the first layer is in contact with the second layer, the second layer is positioned between the first layer and the active layer, the first layer comprises a first carbon nanostructure, and the second layer includes a second carbon nanostructure

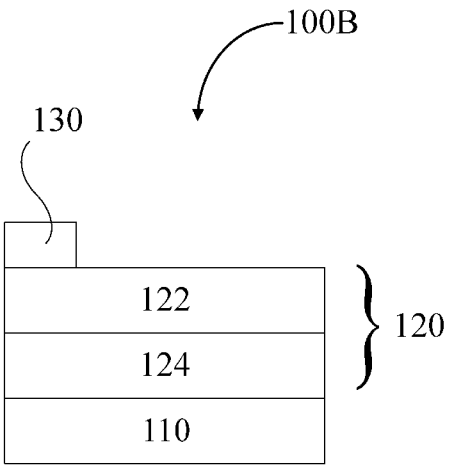

Figure 2

WO 2018/209104 A1

MULTILAYER CARBON NANOTUBE FILM-CONTAINING DEVICES

CROSS-REFERENCE TO RELATED APPLICATIONS

This application claims the benefit of U.S Provisional Patent Application No. 62/504,109 filed May 10, 2017, the contents of which are incorporated herein by reference in their entirety.

CONTRACTUAL ORIGIN

The United States Government has rights in this disclosure under Contract No. DE-AC36-08GO28308 between the United States Department of Energy and Alliance for Sustainable Energy, LLC, the Manager and Operator of the National Renewable Energy Laboratory.

BACKGROUND

The cost of conventional photovoltaics based on silicon modules is now competitive with non-renewable energy sources. Next-generation photovoltaic technologies must offer significantly lower costs or high-value functional properties to extend beyond the current residential rooftop and large-area solar farm markets. Building-integrated photovoltaics – where photovoltaic panels replace conventional building materials such as the roofs, windows, or façades – offer one such alternative pathway to increased solar energy penetration.

SUMMARY

An aspect of the present disclosure is a device that includes an active layer and a first charge transport layer, where the first charge transport layer includes a first layer and a second layer, the first layer is in contact with the second layer, the second layer is positioned between the first layer and the active layer, the first layer comprises a first carbon nanostructure, and the second layer includes a second carbon nanostructure.

In some embodiments of the present disclosure, the first carbon nanotube may include a first single-walled carbon nanotube (SWCNT). In some embodiments of the present disclosure, the first SWCNT may further include a dopant. In some embodiments of the present disclosure, the dopant may include at least one of triethyloxonium hexachloroantimonate, 2,3,5,6-tetrafluoro-7,7,8,8-tetracyanoquinodimethane, a phosphine, an alkyl crown ether complex, an amine, nitrogen, and/or boron. In some embodiments of the present disclosure, the dopant may be present at an atomic concentration between greater than 0% and 30%. In some embodiments of the present disclosure, the first layer may have a thickness between one

nanometer and 200 nm, inclusively. In some embodiments of the present disclosure, the first SWCNT may be at least partially semiconductive and/or partially metallic.

In some embodiments of the present disclosure, the second carbon nanostructure may include a second SWCNT. In some embodiments of the present disclosure, the second SWCNT is not doped. In some embodiments of the present disclosure, the second carbon nanostructure may further include a polymer where the second carbon nanostructure may be at least partially coated by the polymer. In some embodiments of the present disclosure, the polymer may include at least one of poly[(9,9-dioctylfluorenyl-2,7-diyl)-*alt*-*co*-(6,6′-{2,2′-bipyridine})], poly[(9,9-dihexylfluorenyl-2,7-diyl)-*co*-(9,10-anthracene)], poly(9,9-dioctylfluorenyl-2,7-diyl), poly[2-ureido-6[1*H*]-pyrimidinone], poly[(9,9-di-*n*-dodecyl-2,7-fluorendiyl-dimethine)-(1,4-phenylene-dinitrilomethine)], and/or poly(3-hexylthiophene-2,5-diyl) (P3HT). In some embodiments of the present disclosure, the polymer may be present at a mass ratio of the polymer to the second carbon nanostructure between 0.1:1 and 1:1, inclusively. In some embodiments of the present disclosure, the second layer may have a thickness between greater than one nanometer and 200 nm, inclusively. In some embodiments of the present disclosure, the second SWCNT may be at least partially semiconductive and/or partially metallic.

In some embodiments of the present disclosure, the first layer and the second layer are permeable to an intercalating molecule. In some embodiments of the present disclosure, the intercalating molecule may include CH_3NH_2. In some embodiments of the present disclosure, the first layer and the second layer are capable of transmitting light.

In some embodiments of the present disclosure, the first carbon nanostructure may include a first single-walled carbon nanotube (SWCNT) that is doped with 2,3,5,6-tetrafluoro-7,7,8,8-tetracyanoquinodimethane (F_4TCNQ), the F_4TCNQ may be present at an atomic concentration between greater than 0% and 30%, the second carbon nanostructure may include a second SWCNT at least partially coated with poly(3-hexylthiophene-2,5-diyl) (P3HT), the P3HT may be present at a mass ratio of the P3HT to the second SWCNT between 0.1:1 and 1:1, inclusively, and the first layer and the second layer may have a combined thickness between 1 nanometer and 200 nanometers. In some embodiments of the present disclosure, the active layer may include at least one of an inorganic semiconductor material, an organic-inorganic semiconductor material, and/or an organic semiconductor material.

An aspect of the present disclosure is a method for reversibly switching a window integrated photovoltaic device between a first state and a second state, where the method

includes a first reversible transferring of a molecule from a reservoir through at least a charge transport layer to an active layer, intercalating the molecule in the active layer, decalating the molecule from the active layer, and a second reversible transferring of the molecule through at least the charge transport layer to the reservoir. Further, the first reversible transferring results in the first state, while in the first state, the active layer is substantially transparent to visible light, the second reversible transferring results in the second state, while in the second state, the active layer is substantially opaque to visible light, and while in the first state and the second state, the device is capable of converting at least a portion of light to electricity.

In some embodiments of the present disclosure, the charge transport layer may include a first layer and a second layer, the first layer may be in contact with the second layer, the second layer may be positioned between the first layer and the active layer, the first layer may include a first carbon nanostructure, the second layer may include a second carbon nanostructure, and the charge transport layer may be positioned between the active layer and the reservoir.

BRIEF DESCRIPTION OF THE DRAWINGS

Exemplary embodiments are illustrated in referenced figures of the drawings. It is intended that the embodiments and figures disclosed herein are to be considered illustrative rather than limiting.

Figure 1 illustrates a photovoltaic and/or emitting device, according to some embodiments of the present disclosure.

Figure 2 illustrates a photovoltaic and/or light-emitting device having a charge transport layer containing a first layer and a second layer, according to some embodiments of the present disclosure.

Figure 3 illustrates a switchable layer that is reversibly switchable between a first state 310 that is transparent and a second state 320 that is opaque, according to some embodiments of the present disclosure.

Figures 4A, 4B, and 4C illustrate methods for circumventing the tradeoffs found in window-integrated PV (WIPV) devices, according to some embodiments of the present disclosure. Figure 4A illustrates power conversion efficiency as a function of visible transmittance illustrates the fundamental trade-off for semitransparent WIPV using static absorbers. The lower, right marker (marked UV), indicates the maximum theoretical PCE of a PV device

converting only UV light, and the marker labeled IR indicates the maximum PCE of a PV device that converts only IR light. The remaining markers are calculated from the theoretical maximum for a 1.5 eV bandgap methylammonium lead iodide (MAPI) perovskite of varying absorber thicknesses. Figure 4B illustrates AM1.5 solar spectral irradiance as a function of solar photon energy (the outer boundary). The internal spectra correspond to different wavelengths of light with the arrow indicating increasing wavelengths. S-Q is the Shockley–Queisser limit of an absorber layer thick enough to have unity absorption of photons with energy at or above the absorber bandgap. Figure 4C illustrates the intercalation/de-intercalation mechanism behind the photothermal switching of mixed-halide perovskite (MHP) WIPV devices.

Figure 5 illustrates the absorption coefficient as a function of energy for single crystal of methylammonium lead iodide (MAPI), according to some embodiments of the present disclosure.

Figure 6A illustrates a mechanism of the reversible thermal modulation of molecular CH_3NH_2 intercalation in a MAPI film deposited on an ATR crystal, according to some embodiments of present disclosure. Intercalation results in an increase in film thickness ($W_2 > W_1$).

Figure 6B illustrates differential FTIR spectra for two transparent-to-colored WIPV cycles. All spectra are referenced to the initial signal from the $CH_3NH_3PbI_3$ film at 25 °C under vacuum with no CH_3NH_2 present (baseline). A positive peak due to the amine (ν_{N-H}) stretching vibration of the intercalating CH_3NH_2 after 5% partial pressure of CH_3NH_2 was introduced and balanced to atmospheric pressure with Ar. The negative peak highlighted is due to increased film thickness and thus decreased signal from $CH_3NH_3^+$ ions in the detection region of the intercalated film. The film was visibly transparent, which is shown in the optical image to the left of the corresponding spectrum with a dashed white circle that outlines the ATR crystal. Upon heating the ATR crystal to 60 °C with the film in the same atmosphere, the film visually returned to the colored state and the spectrum confirms nearly complete de-intercalation with some residual CH_3NH_2. The stage around the ATR crystal was not heated. The ATR crystal was cooled and heated again in cycle 2 to yield the top two spectra. The spectra are not normalized and are offset for clarity. The background due to thin film interference of each spectrum was subtracted with a polynomial fit.

Figure 7 illustrates background subtraction from FTIR data. The solid line is a 3rd order polynomial fit to the data at 60 °C. The dashed line is a 3rd order polynomial fit to the data at

25 °C. The fit parameters are shown in Figure 7.

Figures 8A-8H illustrate the composition and performance of switchable WIPV devices, according to some embodiments of the present disclosure. Figure 8A illustrates a PV device architecture, according to some embodiments of the present disclosure. Figure 8B illustrates an SEM cross-section image of the device showing the layers beneath the nickel grid coated with PEDDOT:$PSS^{D\text{-}Sorbitol}$, according to some embodiments of the present disclosure. The scale bar is 200 nm. Figure 8C illustrates a photograph of a device with three complete pixels highlighted with dashed white lines, according to some embodiments of the present disclosure. Figure 8D illustrates an SEM image highlighting the nickel grid top contact, according to some embodiments of the present disclosure. The scale bar is 300 μm. Figure 8E illustrates an SEM image of nickel grid coat (white lines) coated with PEDDOT:$PSS^{D\text{-}Sorbitol}$ laminated onto the $SWCNT^{F4TCNQ}$ layer, according to some embodiments of the present disclosure. Excess PEDDOT:$PSS^{D\text{-}Sorbitol}$ is visible along the grid. The scale bar is 50 μm. Figure 8F illustrates an SEM image showing the porous network of $SWCNT^{F4TCNQ}$ that allows gas to permeate through to the $CH_3NH_3PbI_3$ layer for switching, according to some embodiments of the present disclosure. Figure 8G illustrates the transmittance of a device in the transparent (indicated as "bleached") and colored states as a function of wavelength, according to some embodiments of the present disclosure. Figure 8H illustrates the current density as a function of voltage of the champion switchable PV devices in the dark (dashed) and under illumination (solid), according to some embodiments of the present disclosure. The inset table shows PV performance metrics of the device before being transitioned to transparent.

Figure 9 illustrates optical absorption spectra of ink used to generate $SWCNT^{F4TCNQ}$ layer, according to some embodiments of the present disclosure. A SWCNT/PFPD ink was doped in the solution phase with the charge transfer dopant F_4TCNQ at a doping concentration of 250 μg/mL. Adding F_4TCNQ to the SWCNT ink results in bleaching of the S_{11} transitions, indicative of a charge transfer interaction between the dopant and SWCNTs in the solution phase. The ink that was sprayed directly onto the SWCNT/P3HT layer in the device stack.

Figure 10 illustrates the energy diagram of a switchable PV device, according to some embodiments of the present disclosure, according to some embodiments of the present disclosure.

Figure 11 illustrates a comparison of current-voltage characteristics for various device architectures, according to some embodiments of the present disclosure.

Figures 12A, 12B, and 12C illustrate the dynamic transmittance and power generation from switchable WIPV devices, according to some embodiments of the present disclosure. Figure 12A illustrates the short-circuit current as a function of time for 20 cycles of 3 minutes of 1-sun illumination followed by 5 minutes of cooling in the dark. Figure 12B illustrates the short-circuit current as a function of time for the first illumination cycle. The still-frames show the transition from transparent to colored and back to bleached at various times during the process. Figure 12C illustrates the short-circuit current as a function of time for the 15^{th} cycle with corresponding still-frames showing continued device switching.

REFERENCE NUMBERS

100..... device
110..... active layer
120..... charge transport layer
122..... first layer
124..... second layer
130..... charge collecting layer
300..... switchable device
310..... switchable layer in first state
320..... switchable layer in second state
330..... intercalating species reservoir
340..... switching mechanism

DETAILED DESCRIPTION

The present disclosure may address one or more of the problems and deficiencies of the prior art discussed above. However, it is contemplated that some embodiments as disclosed herein may prove useful in addressing other problems and deficiencies in a number of technical areas. Therefore, the embodiments described herein should not necessarily be construed as limited to addressing any of the particular problems or deficiencies discussed herein.

The present disclosure relates to improved photovoltaic devices, photo-emitting devices, and thermochromic devices (examples provided in U.S. Patent Application Publication No. 2017-0089128 A1, which is incorporated herein by reference in its entirety). Figure 1 illustrates a general schematic of such a device 100A that includes an active layer 110 positioned between a first charge transport layer 120A and a second charge transport layer 120B. The device 100A also includes a first charge collecting layer 130A in electrical

communication with the first charge transport layer 120A, and a second charge collecting layer 130B in electrical communication with the second charge transport layer 120B. In some embodiments of the present disclosure, the active layer 110 may absorb light to generate a voltage and/or a current, or the active layer 110 may emit light when a voltage and/or current is applied to the active layer 110. The active layer 110 may include at least one of a bulk inorganic semiconductor layer (silicon, germanium gallium arsenide, cadmium telluride, lead sulfide, etc.), an organic-inorganic semiconductor layer (e.g. methylammonium lead iodide), an organic semiconductor layer (e.g. conjugated polymers such as polyacetylene, phthalocyanine, polyethylene terephthalate, poly(3,4-ethylenedioxythiophene), poly(3-nethyl-thiophene), poly(3-hexylthiophene) and fullerenes (C60, C70, etc.), their derivatives (phenyl-C_{61}-butyric acid methyl ester, thienyl-C_{61}-butyric-acid-methyl ester, etc.), as well as bulk or planar heterojunctions composing a number of these components, and/or semiconductor quantum dots (e.g. silicon, germanium gallium arsenide, cadmium telluride, lead sulfide, cadmium selenide, etc.). The example of Figure 1 illustrates only one active layer 110. However, it is to be understood that a such a device may include one or more active layers, for example, stacked on top of each other to maximize the amount of the sun's energy that is converted to electricity in a photovoltaic device.

In general, a charge transport layer 120 (120A and/or 120B) may be a hole transport layer or an electron transfer layer to enable the generation of charge separation within the device 100. In some embodiments of the present disclosure, at least one of the first charge transport layer 120A and/or the second charge transport layer 120B may include a single-walled carbon nanotube (SWCNT) and/or multi-walled carbon nanotube (MWCNT) layer. As used herein, "CNT" includes SWCNTs and MWCNTs. A CNT layer may be doped and/or wrapped in a polymer. The doping may include immersing the SWCNT network in a solution comprising a charge-transfer dopant until a charge carrier (electron or hole) doping level of the SWCNT network is saturated; e.g. having a carrier density between $1x10^{19}$ and $1x10^{21}$ per cubic centimeter. The charge carrier doping level of the SWCNT network can be further tuned by immersing the SWCNT network in a solvent to intentionally re-dissolve some of the adsorbed dopant. The charge-transfer dopant may include at least one of triethyloxonium hexachloroantimonate (OA, a p-type dopant), 2,3,5,6-Tetrafluoro-7,7,8,8-tetracyanoquinodimethane (F_4TCNQ, a p-type dopant), amines (ammonia, primary, secondary, and tertiary alkyl- or arylamines, n-type dopants), phosphines (n-type dopants), and/or alkali crown ether complexes (n-type dopants). Carbon substitution dopants, such as nitrogen or

boron, may also be employed.

The polymer used for wrapping a CNT may determine the chirality and/or length of the CNT and provide solubility in various solvents. The polymer may also provide energetic alignment to the active layer 110. CNTs may be dispersed in a fluorene-based polymer or co-polymer solution generated by dissolving polymer in toluene and/or an alternative solvent at a concentration between 0.4 – 2 mg/mL. The polymers used may include poly[(9,9-dioctylfluorenyl-2,7-diyl)-*alt*-*co*-(6,6′-{2,2′-bipyridine})] (PFO-BPy), poly[(9,9-dihexylfluorenyl-2,7-diyl)-*co*-(9,10-anthracene)] (PFH-A), poly(9,9-dioctylfluorenyl-2,7-diyl) (PFO), and/or "cleavable" polymers such as poly[2-ureido-6[1*H*]-pyrimidinone] (SMP) and poly[(9,9-di-*n*-dodecyl-2,7-fluorendiyl-dimethine)-(1,4-phenylene-dinitrilomethine)] (PF-PD). Additional polymers may include polythiophenes such as poly(3-hexylthiophene-2,5-diyl) (P3HT). Treatments may be employed to remove the polymer. A solvent soak (e.g. toluene) was used in one example and removed excess fluorene-based polymer or co-polymer, leaving polymer wrapped CNTs in a mass ratio between greater than 0.1:1 and approximately 1:1 (polymer:CNTs), and enabling close physical contact and efficient electronic coupling between CNTs. For "cleavable" polymers, a soak in dilute tri-fluoroacetic acid breaks the bonds in between monomers, enabling complete removal of the polymer.

In general, a charge collecting layer 130 (130A and/or 130B) may be any suitable, highly conductive material that enables the removal of the charges generated in or provided to the active layer 110. In some embodiments of the present disclosure, at least one of the first charge collecting layer 130A and/or the second charge collecting layer 130B may include at least one of the CNT combinations described above for the charge transport layers (120A and 120B) with a higher dopant density. The specific number, combination, and order of the various layers of a specific device will be dictated by the specific use and/or design requirements of the device.

Figure 2 illustrates a schematic of a device 100B that includes an active layer 130 in electrical communication with a charge transport layer 120 having a second layer 124 positioned between the active layer 110 and a first layer 122. The first layer 122 of the charge transport layer 120 may also be in contact with a charge collecting layer 130. In some embodiments of the present disclosure, the first layer 122 may behave like a charge transport layer, while the second layer 122 provides a performance enhancing attribute; e.g. improved band gap alignment, improved charge transport, etc. Examples of such improvements are

provided below. Thus, the first layer 122 may be made from CNTs composed of the elements described above for layers 120A,B and 130A,B for Figure 1. The second layer 124 may be also be composed of these elements. The elements that compose layer 124 combine to provide favorable energetic alignment with the active 1ayer 110 (that is, favored electron (hole) extraction and hole (electron) blocking). The elements that compose layer 122 combine to provide favorable alignment with layer 124 and enhanced lateral carrier transport. The charge collecting layer 130 may include a metallic layer for lateral transport.

Figure 3 illustrates a switchable device 300 having a switchable layer (310 and 320), which may be in the form of a film and/or a layer that may be reversibly switched between a first transparent state 310 to a second tinted state 320, utilizing a switching mechanism 340. Switching of the switchable device 300 between the switchable layers two states (310 and 320) may be induced by an energy input into the device containing the switchable layer (310 and 320) such as solar radiation and/or any other suitable energy source and/or heat source. Other switching mechanisms may include introducing an electrical bias and/or subjecting the switchable device 300 to a mass concentration gradient that drives the intercalating species between the switchable material and the intercalating species reservoir; e.g. by flowing gas over a surface of the switchable material. In some embodiments of the present disclosure, the switchable layer (310 and 320) has been shaped into a specific shape or form, in this example, a film and/or layer. In some embodiments of the present disclosure, the switchable layer (310 and 320) may be in any other suitable shape and/or form; e.g. spheres, cylinders, rods, and/or cones, etc. In addition, the switchable layer (310 and 320) may have at least one textured surface. In the example of Figure 3, the switchable layer (310 and 320) is shown positioned adjacent to an intercalating species reservoir 330. When the switchable layer is in a first transparent state 310, intercalating species 220 are intercalated into the switchable layer 320. As shown in the example of Figure 3, while the switchable layer is in the first transparent state 310, none and/or a fraction of the intercalating species 220 may be contained in an intercalating species reservoir 330. When switched to the second tinted state 320, all or substantially all of the intercalating species 220 may diffuse out of the switchable layer 320 into the intercalating species reservoir 330. However, it should be understood, that in some embodiments of the present disclosure, removal of intercalating species 220 from the switchable layer and/or the intercalating species reservoir 330 may be less than 100% complete; e.g. when the switchable layer is in a first transparent state 310, some intercalating species 220 may remain in the

reservoir 330, and when in a second tinted state 320, some intercalating species 220 may remain in the switchable material.

In some embodiments of the present disclosure, an intercalating species reservoir 330 may be a space positioned adjacent to the switchable layer (310 and 320) such that the space is filled with at least one of a gas, a liquid, and/or a solid. When an intercalating species reservoir 330 includes a space filled with a gas, the space may be at any suitable pressure, from pressures above atmospheric pressure (e.g. about 760 torr up to 1550 torr) to pressures equal to or approaching absolute vacuum (e.g. about 10^{-11} up to 760 torr). In some embodiments of the present disclosure, a gas may be contained in an intercalating species reservoir 330 (e.g. a space) that is completely enclosed and isolated from the environment external to the device 300, with no inlet and/or outlet to allow for the transfer of gas and/or intercalating species 330 between the intercalating species reservoir 330 and an environment external to the device 300. In some embodiments of the present disclosure, at least one port 430 may be positioned within the intercalating species reservoir 330 such that the intercalating species 220 may be reversibly added and/or removed from the intercalating species reservoir 330. In some embodiments of the present disclosure, an intercalating species reservoir 330 in the form of an empty space may be positioned relative to the switchable layer (310 and 320) such that there are no physical barriers to mass-transfer between the space and the switchable layer (310 and 320).

Unlike conventional PV technologies that maximize light absorption through optically dense films, WIPV designs may achieve high solar-to-electrical power conversion efficiency (PCE) while maintaining visible light transmittance (VLT) for acceptable window performance. For this reason, the non-visible regions of the solar spectrum may be targeted for conversion. However, the complex organic materials capable of IR-only conversion constrain these systems to below the thermodynamic limit with a practical PCE limit of 10.8% (see marker labeled IR in Figure 4A), and the ultraviolet (UV) portion of the spectrum makes up only a small fraction of the solar spectrum to provide a theoretical maximum PCE of 2.5% (see marker labeled UV in Figure 4A). As a result, typical WIPV designs feature semitransparent absorber films that are thin enough to absorb only a fraction of the visible spectrum. As shown in Figure 4A for calculations based on methylammonium lead iodide ($CH_3NH_3PbI_3$, MAPI), the ultimate drawback of semitransparent WIPV is that the PCE decreases nearly linearly with VLT. Fewer photons are converted as a perfect absorber (see arrow-head inf Figure 4B), which corresponds to the Shockley–Queisser (S-Q) limit, is reduced to a 10 nm thick absorber (see

tail of the arrow in Figure 4B). Semitransparent WIPV designs thus suffer from the fundamental tradeoff between PCE and VLT.

Thus, as described herein, the tradeoff between PCE and VLT inherent in static absorber materials is circumvented with the demonstration of a "switchable" WIPV device containing an MHP absorber layer that is photothermally modulated between a high-VLT transparent state and a photovoltaic colored state. This is possible due to the low formation energy of MHP materials, which allows for intercalation/de-intercalation of polar molecules with small changes in energy. It is shown herein that this energy can be delivered with sunlight, as shown schematically in Figure 4C. At ambient temperature, molecular intercalation disrupts the MHP structure to yield a transparent state. Upon solar illumination, photothermal heating leads to de-intercalation of the species from the MHP material to yield the relatively opaque, colored photovoltaic state. Cooling reverses the processes by allowing molecules to intercalate back into the MHP that then returns to the transparent state.

Reversible intercalation of methylamine (CH_3NH_2) into MAPI is demonstrated herein using Fourier transform infrared spectroscopy (FTIR) in Figure 6B. MAPI was cast from solution onto an attenuated total reflectance (ATR) crystal to yield a film of thickness W_1, shown schematically in Figure 6A. The film is highlighted with a dashed white circle in the inset optical image (see Figure 6B). The film was sealed in a glass chamber and placed under static vacuum (~40×10^{-3} torr). FTIR signal from this film was then zeroed to give the baseline spectrum in Figure 6B. The atmosphere of the glass chamber was filled with 5% partial pressure of CH_3NH_2 in Ar at atmospheric pressure (~620 torr). The environment was closed, and no more CH_3NH_2 was introduced during the experiment. Introduction of 5% CH_3NH_2 atmosphere caused the MAPI film to bleach (inset image), and CH_3NH_2 ($\nu_{N\text{-}H}$) vibrations emerged from the baseline centered at 3250 cm^{-1} to confirm intercalation of CH_3NH_2 into the MAPI film. The MAPI film increased in thickness as a result of intercalation ($W_2 > W_1$, Figure 6A). Film expansion lead to decreased signal from N-H_x stretching vibrations of methylammonium ($CH_3NH_3^+$) cations in the MAPI film, which was manifested as a negative peak centered at 3130 cm^{-1}.

The transparent-to-colored cycle was completed by heating the ATR crystal to 60 °C, which is similar to the color switching threshold temperature of 68 °C used in vanadium dioxide thermochromic window technology. It is clear from the inset optical images that the film reverted back to the colored state. Signal due to $CH_3NH_3^+$ returned to its baseline level, and the

intensity of the CH_3NH_2 peak was largely reduced due to de-intercalation of CH_3NH_2 from the MAPI film back into the vapor phase, though some residual CH_3NH_2 still remains. A second cycle is displayed to demonstrate repeated reversible switching.

Reversible bleached-to-colored modulation using solar-simulated illumination in a full PV device stack is describe below. A particular challenge was to engineer hole transport and top contact layers that meet four required criteria: *(i)* high electrical conductivity, *(ii)* favorable energetic alignment with the MAPI layer, *(iii)* significant transparency in the visible portion of the solar spectrum, and *(iv)* permeability to CH_3NH_2 vapor. A number of architectures were explored and are summarized in Table 1.

Table 1. Device performance for various hole transport architectures

Hole Transport Architecture	Visibly Transparent	Vapor Permeable	V_{OC} (V)	J_{SC} (mA cm^{-2})	FF (%)	PCE (%)
$SWCNT^{F4TCNQ}$/ $PEDOT:PSS^{D\text{-}Sorbitol}$/Ni Grid	Yes	Yes	0.71 ± 0.24	0.6 ± 0.1	0.19 ± 0.04	0.08 ± 0.02
SWCNT/P3HT/ $PEDOT:PSS^{D\text{-}Sorbitol}$/Ni Grid	Yes	Yes	0.87 ± 0.01	20.7 ± 0.5	0.34 ± 0.06	6.2 ± 1.1
SWCNT/P3HT/$SWCNT^{F4TCNQ}$/$PEDOT:PSS^{D\text{-}Sorbitol}$/Ni Grid	Yes	Yes	0.93 ± 0.01	20.6 ± 0.7	0.54 ± 0.03	10.3 ± 0.9
Spiro-OMeTAD/ $PEDOT:PSS^{D\text{-}Sorbitol}$/Ni Grid*	Yes	Yes	0.96 ± 0.04	0.2 ± 0.1	0.20 ± 0.01	0.04 ± 0.01
Spiro-OMeTAD/Au	No	No	1.05 ± 0.01	21.2 ± 0.3	0.73 ± 0.01	16.3 ± 0.1

As shown herein, four complimentary layers on top of the typical planar MAPI device architecture resulted in optimal performance in both VLT and PCE. A schematic of the full architecture is illustrated in Figure 8A. MAPI was deposited on titanium dioxide (using established methods) as the electron transport layer and fluorine-doped tin oxide as the transparent bottom contact. The MAPI was coated with a hole transport layer of single-walled carbon nanotubes wrapped in poly(3-hexylthiophene) (SWCNT/P3HT). This layer is porous, visibly transparent, and is a promising alternative to 2,2′,7,7′-Tetrakis(*N*,*N*-di-*p*-methoxyphenylamine)-9,9′-spirobifluorene (spiro-OMeTAD). Spiro-OMeTAD enables excellent PV performance but leads to degradation of the MAPI absorber in PV devices. A second layer of SWCNTs doped with 2,3,5,6-Tetrafluoro-7,7,8,8-tetracyanoquinodimethane

($SWCNT^{F4TCNQ}$) was spray-coated to improve lateral electrical transport to the top contact. F4TCNQ is a charge-transfer dopant that enhances p-type conductivity within each SWCNT (see Figure 9). This layer was also chemically treated with trifluoroacetic acid after deposition to de-polymerize and remove the wrapping polymer that provides solubility in order to enhance electrical conductivity between SWCNTs. An electrical contact to the top of conventional MHP PV devices was made with evaporated metal. A nickel micromesh was laminated to provide high electrical conductivity and 88% optical transparency. The nickel mesh was laminated to the $SWCNT^{F4TCNQ}$ layer by first spray-coating poly(3,4-ethylene dioxythiophene):poly(styrenesulfonate), an electrically conductive polymer, doped with D-sorbitol ($PEDOT:PSS^{D\text{-}Sorbitol}$) that serves as an "electric glue" between the $SWCNT^{F4TCNQ}$ and the micromesh. The nickel micromesh was then adhered to the $SWCNT^{F4TCNQ}$ layer with gentle mechanical pressure to complete the PV device. The $PEDOT:PSS^{D\text{-}Sorbitol}$ layer functions as an effective hole transport layer. The energy diagram describing the full device architecture is illustrated in Figure 10.

The two layers of SWCNTs are important to the function of the double-layer SWCNT layer described above. As shown in Table 1, if only the doped SWCNT layer is in contact with the perovskite active layer, the power conversion efficiency is extremely low and the device does not function well at all. However, when the undoped SWCNT layer (the second layer 124 of Figure 2) is used in between the heavily doped (conductive) layer (the first layer 122 of Figure 2) and the perovskite active layer (active layer 110 of Figure 2), the device functions very well, with power conversion efficiency exceeding 10%. Thus, the undoped SWCNT layer (second layer 124) appears to provide the appropriate energy level matching and charge extraction from the device active layer 110, after which the charge lifetime in the undoped layer is very long. This allows the charges to diffuse to the conductive SWCNT layer (the first layer 122) where they can be extracted to the charge collecting layer 130, into the external circuit as current. This allows for many variations on this double-layer electrode. The undoped layer (the second layer 124) can be highly enriched semiconducting SWCNTs or mixed (metallic and semiconducting) SWCNTs, as long as they are not doped sufficiently to have high carrier density; e.g. less than about $1x10^{17}$ per cubic centimeter. Any number of polymers and/or surfactants may be used to generate this layer, as long as the polymers/surfactants does/do not dope the SWCNTs. The conductive SWCNT layer (the first layer 122) may also include any ratio of semiconducting to metallic SWCNTs, as long as they are sufficiently doped; e.g. having

a carrier density between $1x10^{19}$ and $1x10^{21}$ per cubic centimeter. Any number of different diameters and diameter distributions can also be used to produce both of the layers, with the full range of commonly synthesized SWCNT diameters being feasible (between 0.6 nm and 2.0 nm).

Figure 8B illustrates a scanning electron microscopy (SEM) image of the device cross-section. A 600 nm-thick MAPI absorber layer was deposited on a 100 nm-thick layer of TiO_2. The two SWCNT layers formed a continuous and wispy layer of approximately 100 nm. The SWCNT/P3HT polymer-containing layer cannot be distinguished from the $SWCNT^{F4TCNQ}$ doped layer in the image. Details regarding chirality/diameter distributions are supplied below for these two distinct SWCNT layers. Figure 8C illustrates a photograph highlighting three pixels (dashed white boxes) completed with the nickel microgrid top contact. Continuous adhesion of the nickel microgrid is shown in Figure 8D, with the exception of where the device was cross-sectioned in the foreground of the SEM image. Figure 8E is an SEM image that highlights excess $PEDOT:PSS^{D\text{-}Sorbitol}$ that is also beneath the nickel microgrid layer to adhere it to the $SWCNT^{F4TCNQ}$ layer. Figure 8F is an SEM image illustrating the porosity of the SWNT layers, which is needed for CH_3NH_2 vapor permeation into the MAPI layer.

VLT is an important metric for WIPV devices. Figure 8G shows the transmittance of the full device stack spanning UV to IR portions of the electromagnetic spectrum. The visible portion is highlighted to illustrate reversible switching in this region. The device was highly absorbing in the visible portion in the colored state with an average VLT of 3%, which is a standard upper limit needed for building occupant comfort from direct sun glare. The VLT increased to 68% when in the transparent state (5% pressure CH_3NH_2 in argon at room temperature). The observed decrease in transmittance in the infrared region is due to thin film interference and FTO absorption that is featured in current low-emissivity films used in current high-performance window technology.

Figure 8H shows the current density – voltage curve of the switchable PV device in the dark (dashed) and under 1-sun illumination (solid). The champion device exhibited a PCE of 11.3% with an average of $10.3 \pm 0.9\%$ in five devices. A table with the performance metrics of the high-performing device are shown in the inset to Figure 8H. For comparison, control devices were fabricated with the same MHP and electron contact layers but with Li-doped spiro-OMeTAD as the hole transport layer and gold as the top contact to mimic conventional MHP PV devices. The control devices, which do not switch since the gold contact is not

permeable to CH_3NH_2 vapor, exhibited an average PCE of 16.3 ± 0.1%. The short-circuit current density (J_{SC}) of 21.2 mA cm^{-2} for the champion switchable device was identical to the control device, whereas deficits in the open-circuit voltage (V_{OC}) and fill factor (FF) characterize the switchable WIPV device compared to the control device. The $SWCNT^{F4TCNQ}$ layer significantly improves FF, which is only 0.34 ± 0.06% for devices with the SWCNT/P3HT and not including the $SWCNT^{F4TCNQ}$ layer. The SWCNT/P3HT alone was too electrically resistive for transport to the nickel micromesh contacts. The $SWCNT^{F4TCNQ}$ layer significantly reduced the series resistance (see Figure 11).

Figures 12A-12C show dynamic photothermal modulation of a WIPV device transmittance under 1-sun illumination while generating photocurrent. Figure 12A is a plot of short-circuit current output as a function of time for a device enclosed in an atmosphere 5% CH_3NH_2 balanced with argon to atmospheric pressure. The device started in the intercalated (transparent) state at time zero until the device was exposed to 1-sun solar-simulated illumination at 30 seconds, indicated by gray boxes in Figure 12A. Current was immediately observed from the device after illumination, which increased and started to plateau after 1 minute. The current dropped to zero when the lamp was turned off after three minutes. The lamp was turned back on after five minutes, and this cycle was repeated 20 times in a closed atmosphere (no additional CH_3NH_2) to demonstrate repeated cycling.

Reversible color change was achieved during each of these cycles, as demonstrated by still-frame images taken during the first and fifteenth cycles (see Figures 12B and 12C and inset of Figure 12C). The current kinetics were similar in each cycle. The device immediately produced current when illuminated, but did not visibly exhibit color change. The current increased at a near-linear rate until 40 seconds of illumination when the current increased at a higher rate, which correlated to visible color change and complete switching after three minutes. When the lamp was turned off, the device cooled in the chamber, which caused CH_3NH_2 vapor to intercalate back into the MAPI and return the device to the transparent state after 3 minutes.

Maximum current decreased monotonically from nearly 1 mA to 0.18 mA after 20 cycles. The still-frame images in Figure 12C suggest degradation of the MAPI layer, which show the device no longer had consistent coloration across the device as it did on the first cycle. Without wishing to be bound by theory, there are a number of explanations for this: *(i)* It is possible the MAPI layer does not re-form into the same uniform morphology as the original to

yield a thinner, more transparent layer. *(ii)* Ions are known to migrate at elevated temperatures and react with other layers in the device. *(iii)* Decreased sublimation temperature has been observed previously for methylammonium halides when complexed to PbI_2, so components of MAPI may have been lost to the gas phase to yield PbI_2 in the layer. It should be possible to overcome imperfect irreversibility with additional engineering and understanding of the film intercalation/de-intercalation dynamics.

As described above, a device may include a transport layer having one more layers constructed of CNT, for example SWCNT. CNTs may be chosen to have a characteristic diameter, length, and/or chirality. For example, CNTs may have a diameter between 0.4 nm and 40 nm. CNTs may also have a characteristic diameter to length ratio as high as 1.3 * 10^8. A layer used to construct a transport layer may have a thickness between 5 nm and 500 nm. In addition, CNTs may be selected having one or more characteristic chiralities.

Materials and Methods:

PCE versus VLT calculations: The calculations shown in Figure 4A were done with Mathematica code written by Steven Byrnes and modified to read in the absorption coefficient of an arbitrary absorber and calculate PCE as a function of solar photon energy. The absorption coefficient, $\alpha(E)$, of a MAPI single crystal was determined using ellipsometry and was used for calculations for different absorber layer thickness. An optical bandgap of 1.5 eV is used for the S-Q limit. Because we are evaluating a window technology, we assume one pass of light through the absorber to give the number of photons absorbed:

$$a(E,W) = \Gamma(E)(1 - \exp[-\alpha(E)W])$$

where $\Gamma(E)$ is the AM1.5 solar spectrum, E is the solar photon energy, and W is the thickness of the absorber layer. The absorbance is used to calculate the current density from the device from the following equation:

$$J = e\int_{E_1}^{E_2}\left(a(E,W) - R_0(E,V)\exp\left[\frac{e\,V}{k_B\,T} - 1\right]\right)dE$$

where e is the elementary charge, R_0 is the radiative recombination rate at zero quantum Fermi level splitting, V is voltage, and k_B is the Boltzmann constant. The PCE is then calculated from the maximum power point (i.e. where the product of J and V reaches a maximum).

Visible light transmittance is calculated from the following:

$$VLT = \int_{E_1}^{E_2} 1 - \frac{a(E,W)}{\Gamma(E)}\, dE$$

where visible light is defined by what the human eye can see, which is between $E_1 = 1.65$ eV and $E_2 = 3.26$ eV.

Crystal structures: Crystal structures in Figure 4C were for illustrative purposes only, as the actual structure of the intercalated MAPI was not determined. The images were generated from a .cif file of hydrated MAPI ($CH_3NH_3PbI_3 \cdot H_2O$) using Jmol open-source software. Hydrogen is not shown.

Absorber layer solution: The solution used to solubilize MAPI precursors was obtained by charging acetonitrile with CH_3NH_2 gas. Acetonitrile was dried and de-gassed using three freeze-pump-thaw cycles and placed in an air-tight flask. CH_3NH_2 gas was flown into the vessel through a Schlenk-line assembly. The acetonitrile was charged until a 30% by volume CH_3NH_2 solution was achieved. The flask was sealed and stored in a -20 °C freezer. Solution was removed with needle through septum to keep the solution isolated from air exposure.

FTIR measurements: A Bruker Alpha FTIR spectrometer outfitted with a diamond ATR crystal attachment was used in the study. A MAPI film was deposited onto an ATR crystal by drop-casting a 0.055 M solution composed of methylammonium iodide and PbI_2 (5% excess) and the 30% CH_3NH_2 in acetonitrile solution. The film was annealed at 100 °C for 30 minutes. Securing a custom glass chamber over the ATR crystal stage with a Viton O-ring enclosed the film. Superglue was added to the O-ring/ATR stage interface to ensure the seal was maintained at atmospheric pressure. The film was pumped down with a roughing pump over night to obtain a base pressure of 68 mtorr. CH_3NH_2 was introduced into the glass jar at 20 torr, which bleached the MAPI film. The jar was balanced with argon to reach atmospheric pressure. The temperatures reported are those measured and delivered to the ATR stage with OPUS 7.2 software. Spectra shown at 60 °C were taken after the 3 minutes it took to ramp to that temperature. Spectra shown at 25 °C were taken after 21 minutes, which is the time took to cool to that temperature. The backgrounds of the resulting spectra were non-linear due to thin film diffraction due to change in the MAPI film thickness. The background was subtracted using a 3rd order polynomial fit using IGOR Pro version 6.37. One fit was used to subtract the baseline at each temperature. The raw data and polynomial fits are shown in Figure 7.

Photothermal switching of MAPI film: Glass was cut into a 1 inch×1 inch square, sonicated in

acetone for 15 minutes, and blown dry with dry air. The substrates were treated in a UV-ozone cleaner for 15 minutes before spin-coating a 0.55 M solution composed of methylammonium iodide and PbI_2 (5% excess) and the 30% CH_3NH_2 in acetonitrile solution onto the substrate at 2000 rpm for 20 s. The film was annealed at 100 °C for 30 minutes on a hotplate. Photothermal switching of MAPI films was measured in a custom-built glass chamber outfitted with optical ports and feedthroughs for gas input/output and a pressure gauge. The glass substrate with MAPI film was secured in the chamber with a clip facing the optical port. The chamber is sealed with a Viton o-ring and clamp and pumped down over night to reach a base pressure of 40 mtorr measured with a Varian type 0531 vacuum gauge. 5% CH_3NH_2 partial pressure is introduced into the chamber and backfilled with argon to reach slight overpressure above atmospheric pressure (enough pressure to bubble Ar through 4 inches of mercury in a 1-inch tube). A Cole-Palmer Illuminator 41720-series is used for solar-simulated illumination. The lamp simulates 1-sun conditions by adjusting the intensity to 1000 W m^{-2} using a Newport power meter (model 841-PE) with a model 818P-015-19 sensor head.

SWCNT/P3HT ink preparation: Powdered Powdered SWCNTs produced by the CoMoCAT process, SWeNT CG200, were purchased from Sigma-Aldrich. The producers of this material report a diameter range of 0.7−1.4 nm and a relative purity of 90% as the percentage of carbon that is present as SWNTs. rr-P3HT (3.0 mg, Rieke Metals Inc., weight-average molecular weight M_w = 50000 g mol^{-1}, and regioregularity = 95%) was dissolved in 5.00 mL of chlorobenzene and sonicated in a bath sonicator for 60 min. SWCNTs (2.5 mg) were added, as purchased, to the dissolved polymer solution and treated with a Cole Parmer 750 W ultrasonic probe, operating at 100% power, for 10 min. After sonication, 5 mL of chlorobenzene was added to improve the solubility of the polymer−nanotube hybrids. The mixture was subsequently centrifuged for 8 minutes at 10000g (Beckman Coulter ultracentrifuge, SW32 rotor) to remove unfunctionalized SWCNTs and other carbonaceous particles. The precipitate was discarded, and the supernatant was recovered. 10 mL toluene was added in order to remove the excess polymer. The mixture was then mildly heated for 60 minutes to induce aggregation of the functionalized SWNTs. The aggregates were then removed by centrifugation (4 minutes at 16000g). The supernatant containing excess polymer was discarded, and the precipitate was recovered. The pellet consisted of 1.5−1.6 mg of polymer-wrapped nanotubes, which were dispersed in 6 mL of chloroform. Immediately prior to spin-coating, the chloroform dispersion was sonicated with an ultrasonic probe for 1 minute at low intensity (~10% of amplitude) to break up clusters and bundles.

$SWCNT^{F4TCNQ}$ ink preparation: SWCNTs were synthesized in-house at NREL via laser vaporization of a graphite target at a furnace temperature of 1125 °C. The imine-based dispersing polymer, poly[(9,9-di-n-dodecyl-2,7-fluorendiyl-dimethine)-(1,4-phenylene-dinitrilomethine)] (PFPD), was synthesized in-house using procedures known to one of ordinary skill in the art. To disperse the SWCNTs, 1.4 mg mL^{-1} SWCNTs and 2 mg mL^{-1} PFPD were added to toluene and processed using an ultrasonic probe for 15 min while the vial was submerged in a bath of dry ice and methanol. Following ultrasonication, the undispersed material is pelleted out via 5 min ultracentrifugation (13,200 rpm, 20°C) using a Beckman Coulter SW32Ti motor. The supernatant was retained and underwent further ultracentrifugation (20 hr, 24,100 rpm, 0°C) to remove excess PFPD. The resulting pellet, containing highly enriched semiconducting SWCNTs wrapped with PFPD (SWCNT/PDPD), was re-dispersed in neat toluene. The SWCNT/PDPD ink was doped in solution phase by adding 250 µg/mL using 2,3,5,6-Tetrafluoro-7,7,8,8-tetracyanoquinodimethane (F_4TCNQ). The bleach of the S_{11} transition in the optical absorption spectrum of the ink after adding F4TCNQ indicates successful doping (see Figure 9).

Device fabrication: Substrates with pre-patterned FTO deposited on glass were purchased from Thin Film Devices, Inc. The substrates were sonicated in acetone for 15 minutes and blown dry with dry air. The substrates were treated in a UV-ozone cleaner for 15 minutes before spin-coating a 0.15 M TAA solution in 1-butanol (TAA= titanium diisopropoxide bis(acetylacetonate, 75 wt% in 2-propanol, concentration of ~2 M) at 700 rpm for 10 s, followed by 1000 rpm for 10 s, and finally 2000 rpm for 30 s. The resulting film is placed on a hot plate at 125 °C for >2 minutes to drive off solvent and then placed in a 500 °C furnace to sinter into TiO_2. A 0.55 M solution composed of methylammonium iodide and PbI_2 (5% excess) and the 30% CH_3NH_2 in acetonitrile solution was spin-coated onto the substrate at 2000 rpm for 20 s in an inert atmosphere glovebox. The film was annealed at 100 °C for 30 minutes in the glovebox to yield a MAPI layer. The SWCNT/P3HT were deposited onto the MAPI layer by spinning the substrate at 3000 rpm and dropping 300 µL of the SWCNT/P3HT dispersion at a rate of ~1 drop every 3 seconds. $SWCNT^{F4TCNQ}$ thin films were deposited onto the WIPV using ultrasonic spray deposition. Briefly, MAPI films on TiO_2/glass substrates were heated to 130 °C on the stage in the spray chamber. Then, the $SWCNT^{F4TCNQ}$ ink was sprayed using a dispersion flow rate of 0.25 mL/min, gas flow rate of 7.0 std L/min, and nozzle power at 0.8 W for 30 coats. After deposition, the films were soaked at 80 °C in a solution of 10 µL/mL of trifluoroacetic acid (Sigma-Aldrich) in toluene for 30 seconds, followed by a rinse in neat

toluene to fully remove the wrapping polymer, PFPD. Nickel micromesh composed of a square network of 14 μm×14 μm nickel bars with 268 μm×268 μm holes was purchased from Precision Eforming, Inc. A 2-inch×4-inch piece of mesh was attached to an aluminum plate using polyimide tape. The aluminum plate is attached to a hotplate with polyimide tape and set to 120 °C. PEDOT:PSS (CLEVIOS PH1000) was purchased from Heraeus. 3 mL of PEDOT:PSS was combined with 450 mg D-sorbitol and 136 μL dimethylsulfoxide and stirred with a magnetic stir bar for 15 minutes. The solution was sprayed onto the micromesh on the hotplate using an airbrush (Master Airbrush Model S68). The PEDOT layer is sprayed with 10 passes at a rate of ~1 inch s^{-1} at a distance of 6 inches from the mesh with the airbrush throttle fully open. The PEDOT:$PSS^{D\text{-}Sorbitol}$ was annealed for 10 minutes after spraying and then cooled to room temperature before being cut into ~3 mm×11 mm strips. Transferring the strips with a tweezers to cover the active area and pressing with gentle finger pressure through a flexible Polyethylene terephthalate substrate completes the switchable PV device.

UV-vis-NIR measurements: Measurements were carried out on a Cary-6000i spectrometer with an integrating sphere attachment. Devices were scored and cracked to roughly 2 cm wide to fit into cuvettes. Silicone oil was placed on the back-side of the device to adhere it to the cuvette and avoid additional thin film interference. The cuvette was sealed with a septum, and the atmosphere was removed with a roughing pump through a needle. For the bleached state measurement, 5% CH_3NH_2 partial pressure was added to the cuvette and backfilled with argon. The cuvette was filled with argon for the colored state measurement.

Current-voltage measurements: Solar cell devices were measured under AM1.5 illumination in an inert atmosphere using a Newport solar simulator calibrated with a Si photodiode (Hamamtsu, S1787–04). An aperture of 0.06 cm^2 was used when measuring current-voltage curves.

Photocurrent measurement in switching device: Dynamic photoresponse of PV devices was measured in a custom-built glass chamber outfitted with optical ports, feedthroughs for gas input/output, electrical connection, and a pressure gauge. A PV device was secured in the chamber with a clip, and electrical connection to the device was made with alligator clips. The electrical connections are fed through the chamber to a Kiethley 2400 sourcemeter interfaced to a computer using Labtracer 2.0 software. The chamber is sealed with a Viton o-ring and clamp and pumped down over night to reach a base pressure of 40 mtorr measured with a Varian type 0531 vacuum gauge. 5% CH_3NH_2 partial pressure is introduced into the chamber

and backfilled with argon to reach slight overpressure above atmospheric pressure (enough pressure to bubble Ar through 4 inches of mercury in a 1-inch tube). A Cole-Palmer Illuminator 41720-series is used for solar-simulated illumination. The lamp simulates 1-sun conditions by adjusting the intensity and monitoring the short-circuit current of the device until it matches the short-circuit current of the device measured in the calibrated Newport solar simulator.

Examples:

Example 1. A device comprising: an active layer; and a first charge transport layer, wherein: the first charge transport layer comprises a first layer and a second layer, the first layer is in contact with the second layer, the second layer is positioned between the first layer and the active layer, the first layer comprises a first carbon nanostructure, and the second layer comprises a second carbon nanostructure.

Example 2. The device of Example 1, wherein the first carbon nanostructure comprises a first carbon nanotube (CNT).

Example 3. The device of either Example 1 or Example 2, wherein the first CNT comprises a first single-walled carbon nanotube (SWCNT).

Example 4. The device of any one of Examples 1-3, wherein the first SWCNT has a diameter between 0.4 nm and 40 nm, inclusively.

Example 5. The device of any one of Examples 1-4, wherein the first CNT further comprises a dopant.

Example 6. The device of any one of Examples 1-5, wherein the dopant comprises at least one of triethyloxonium hexachloroantimonate, 2,3,5,6-tetrafluoro-7,7,8,8-tetracyanoquinodimethane (F_4TCNQ), a phosphine, an alkyl crown ether complex, an amine, nitrogen, or boron.

Example 7. The device of any one of Examples 1-6, wherein the dopant is F_4TCNQ.

Example 8. The device of any one of Examples 1-7, wherein the dopant is present at an atomic concentration between greater than 0% and 30%.

Example 9. The device of any one of Examples 1-8, wherein the dopant provides a carrier density greater than $1x10^{17}$ per cubic centimeter.

Example 10. The device of any one of Examples 1-9, wherein the carrier density is between $1x10^{19}$ and $1x10^{21}$ per cubic centimeter

Example 11. The device of any one of Examples 1-10, wherein the first layer has a thickness between one nanometer and 200 nm, inclusively.

Example 12. The device of any one of Examples 1-11, wherein the thickness is between 10 nm and 100 nm, inclusively.

Example 13. The device of any one of Examples 1-12, wherein the first CNT is at least partially semiconductive or partially metallic.

Example 14. The device of any one of Examples 1-13, wherein the first CNT is partially semiconductive and partially metallic.

Example 15. The device of any one of Examples 1-14, wherein the second carbon nanostructure comprises a second CNT.

Example 16. The device of any one of Examples 1-15, wherein the second CNT comprises a second SWCNT.

Example 17. The device of any one of Examples 1-16, wherein the second SWCNT has a diameter between 0.4 nm and 40 nm, inclusively.

Example 18. The device of any one of Examples 1-17, wherein the second SWCNT is not doped.

Example 19. The device of any one of Examples 1-18, wherein the second SWCNT further comprises a dopant providing a carrier density less than $1x10^{17}$ per cubic centimeter.

Example 20. The device of any one of Examples 1-19, wherein: the first carbon nanostructure further comprises a polymer, and the first carbon nanostructure is at least partially coated by the polymer.

Example 21. The device of any one of Examples 1-20, wherein: the second carbon nanostructure further comprises a polymer, and the second carbon nanostructure is at least partially coated by the polymer.

Example 22. The device of any one of Examples 1-21, wherein the polymer comprises at least one of poly[(9,9-dioctylfluorenyl-2,7-diyl)-*alt*-*co*-(6,6′-{2,2′-bipyridine})], poly[(9,9-dihexylfluorenyl-2,7-diyl)-*co*-(9,10-anthracene)], poly(9,9-dioctylfluorenyl-2,7-diyl), poly[2-ureido-6[1*H*]-pyrimidinone], poly[(9,9-di-*n*-dodecyl-2,7-fluorendiyl-dimethine)-(1,4-phenylene-dinitrilomethine)], or poly(3-hexylthiophene-2,5-diyl) (P3HT).

Example 23. The device of any one of Examples 1-22, wherein the polymer is P3HT.

Example 24. The device of any one of Examples 1-23, wherein the polymer is present at a mass ratio of the polymer to the second carbon nanostructure between 0.1:1 and 1:1, inclusively.

Example 25. The device of any one of Examples 1-24, wherein the second layer has a thickness between greater than one nanometer and 200 nm, inclusively.

Example 26. The device of any one of Examples 1-25, wherein the thickness is between 10 nm and 100 nm, inclusively.

Example 27. The device of any one of Examples 1-26, wherein the first layer and the second layer have a combined thickness between greater than 1 nanometer and 200 nm, inclusively.

Example 28. The device of any one of Examples 1-27, wherein the combined thickness is between 10 nm and 100 nm, inclusively.

Example 29. The device of any one of Examples 1-28, wherein the second CNT is at least partially semiconductive or partially metallic.

Example 30. The device of any one of Examples 1-29, wherein the second CNT is partially semiconductive and partially metallic.

Example 31. The device of any one of Examples 1-30, wherein the first layer and the second layer are permeable to an intercalating molecule.

Example 32. The device of any one of Examples 1-31, wherein the intercalating molecule comprises CH_3NH_2.

Example 33. The device of any one of Examples 1-32, wherein the first layer and the second layer are capable of transmitting light.

Example 34. The device of any one of Examples 1-33, wherein: the first carbon nanostructure comprises a first single-walled carbon nanotube (SWCNT) that is doped with 2,3,5,6-tetrafluoro-7,7,8,8-tetracyanoquinodimethane (F_4TCNQ), the F_4TCNQ is present at an atomic concentration between greater than 0% and 30%, the second carbon nanostructure comprises a second SWCNT at least partially coated with poly(3-hexylthiophene-2,5-diyl) (P3HT), the P3HT is present at a mass ratio of the P3HT to the second SWCNT between 0.1:1 and 1:1, inclusively, and the first layer and the second layer have a combined thickness between 1 nanometer and 200 nanometers.

Example 35. The device of any one of Examples 1-34, wherein the active layer comprises at least one of an inorganic semiconductor material, an organic-inorganic semiconductor material, or an organic semiconductor material.

Example 36. The device of any one of Examples 1-35, wherein the inorganic semiconductor material comprises at least one of silicon, germanium, gallium, arsenic, cadmium, tellurium, lead, or sulfur.

Example 37. The device of any one of Examples 1-36, wherein the organic-inorganic semiconductor material comprises a perovskite.

Example 38. The device of any one of Examples 1-37, wherein the perovskite comprises methylammonium lead iodide.

Example 39. The device of any one of Examples 1-38, wherein the organic semiconductor material comprises at least one of polyacetylene, phthalocyanine, polyethylene terephthalate, poly(3,4-ethylenedioxythiophene), poly(3-nethyl-thiophene), poly(3-hexylthiophene) a fullerene, or a fullerene derivative.

Example 40. The device of any one of Examples 1-39, further comprising a charge collecting layer, wherein the first layer is positioned between the second layer and the charge collecting layer.

Example 41. The device of any one of Examples 1-40, wherein the charge colleting layer comprises a metal.

Example 42. The device of any one of Examples 1-41, wherein the metal comprises nickel.

Example 43. The device of any one of Examples 1-42, wherein the metal is capable of transmitting light.

Example 44. The device of any one of Examples 1-43, wherein the metal is configured as a mesh having openings comprising a characteristic diameter of up to 300 nanometers.

Example 45. The device of any one of Examples 1-44, further comprising a layer of PEDOT:PSS$^{D\text{-}Sorbitol}$, wherein the PEDOT:PSS$^{D\text{-}Sorbitol}$ electrically connects the charge collecting layer to the first layer.

Example 46. The device of any one of Examples 1-45, further comprising a second charge transport layer, wherein the active layer is positioned between the second layer and the second charge transport layer.

Example 47. The device of any one of Examples 1-46, wherein the second charge transport layer comprises titanium dioxide.

Example 48. The device of any one of Examples 1-47, wherein the device is capable of transmitting visible light through the device.

Example 49. The device of any one of Examples 1-48, further comprising a reservoir containing an intercalating molecule, wherein the first charge transport layer is positioned between the active layer and the reservoir.

Example 50. A method for reversibly switching a window integrated photovoltaic device between a first state and a second state, the method comprising: a first reversible transferring of a molecule from a reservoir through at least a charge transport layer to an active layer; intercalating the molecule in the active layer; decalating the molecule from the active layer; and a second reversible transferring of the molecule through at least the charge transport layer to the reservoir, wherein: the first reversible transferring results in the first state, while in the first state, the active layer is substantially transparent to visible light, the second reversible transferring results in the second state, while in the second state, the active layer is substantially opaque to visible light, and while in the first state and the second state, the device is capable of converting at least a portion of light to electricity.

Example 51. The method of Example 50, wherein: the charge transport layer comprises a first layer and a second layer, the first layer is in contact with the second layer, the second layer is positioned between the first layer and the active layer, the first layer comprises a first carbon nanostructure, the second layer comprises a second carbon nanostructure, and the charge transport layer is positioned between the active layer and the reservoir.

The foregoing discussion and examples have been presented for purposes of illustration and description. The foregoing is not intended to limit the aspects, embodiments, or configurations to the form or forms disclosed herein. In the foregoing Detailed Description for example, various features of the aspects, embodiments, or configurations are grouped together in one or more embodiments, configurations, or aspects for the purpose of streamlining the disclosure. The features of the aspects, embodiments, or configurations, may be combined in alternate aspects, embodiments, or configurations other than those discussed above. This method of disclosure is not to be interpreted as reflecting an intention that the aspects, embodiments, or configurations require more features than are expressly recited in each claim.

Rather, as the following claims reflect, inventive aspects lie in less than all features of a single foregoing disclosed embodiment, configuration, or aspect. While certain aspects of conventional technology have been discussed to facilitate disclosure of some embodiments of the present invention, the Applicants in no way disclaim these technical aspects, and it is contemplated that the claimed invention may encompass one or more of the conventional technical aspects discussed herein. Thus, the following claims are hereby incorporated into this Detailed Description, with each claim standing on its own as a separate aspect, embodiment, or configuration.

CLAIMS

What is claimed is:

1. A device comprising:
an active layer; and
a first charge transport layer, wherein:
the first charge transport layer comprises a first layer and a second layer,
the first layer is in contact with the second layer,
the second layer is positioned between the first layer and the active layer,
the first layer comprises a first carbon nanostructure, and
the second layer comprises a second carbon nanostructure.

2. The device of claim 1, wherein the first carbon nanotube comprises a first single-walled carbon nanotube (SWCNT).

3. The device of either claim 1 or claim 2, wherein the first SWCNT further comprises a dopant.

4. The device of any one of claims 1-3, wherein the dopant comprises at least one of triethyloxonium hexachloroantimonate, 2,3,5,6-tetrafluoro-7,7,8,8-tetracyanoquinodimethane, a phosphine, an alkyl crown ether complex, an amine, nitrogen, or boron.

5. The device of any one of claims 1-4, wherein the dopant is present at an atomic concentration between greater than 0% and 30%.

6. The device of any one of claims 1-5, wherein the first layer has a thickness between one nanometer and 200 nm, inclusively.

7. The device of any one of claims 1-6, wherein the first SWCNT is at least partially semiconductive or partially metallic.

8. The device of any one of claims 1-7, wherein the second carbon nanostructure comprises a second SWCNT.

9. The device of any one of claims 1-8, wherein the second SWCNT is not doped.

10. The device of any one of claims 1-9, wherein:

the second carbon nanostructure further comprises a polymer, and

the second carbon nanostructure is at least partially coated by the polymer.

11. The device of any one of claims 1-10, wherein the polymer comprises at least one of poly[(9,9-dioctylfluorenyl-2,7-diyl)-*alt*-*co*-(6,6′-{2,2′-bipyridine})], poly[(9,9-dihexylfluorenyl-2,7-diyl)-*co*-(9,10-anthracene)], poly(9,9-dioctylfluorenyl-2,7-diyl), poly[2-ureido-6[1*H*]-pyrimidinone], poly[(9,9-di-*n*-dodecyl-2,7-fluorendiyl-dimethine)-(1,4-phenylene-dinitrilomethine)], or poly(3-hexylthiophene-2,5-diyl) (P3HT).

12. The device of any one of claims 1-11, wherein the polymer is present at a mass ratio of the polymer to the second carbon nanostructure between 0.1:1 and 1:1, inclusively.

13. The device of any one of claims 1-12, wherein the second layer has a thickness between greater than one nanometer and 200 nm, inclusively.

14. The device of any one of claims 1-13, wherein the second SWCNT is at least partially semiconductive or partially metallic.

15. The device of any one of claims 1-14, wherein the first layer and the second layer are permeable to an intercalating molecule.

16. The device of any one of claims 1-15, wherein the intercalating molecule comprises CH_3NH_2.

17. The device of any one of claims 1-16, wherein the first layer and the second layer are capable of transmitting light.

18. The device of any one of claims 1-17, wherein:

the first carbon nanostructure comprises a first single-walled carbon nanotube (SWCNT) that is doped with 2,3,5,6-tetrafluoro-7,7,8,8-tetracyanoquinodimethane (F_4TCNQ),

the F_4TCNQ is present at an atomic concentration between greater than 0% and 30%,

the second carbon nanostructure comprises a second SWCNT at least partially coated with poly(3-hexylthiophene-2,5-diyl) (P3HT),

the P3HT is present at a mass ratio of the P3HT to the second SWCNT between 0.1:1 and 1:1, inclusively, and

the first layer and the second layer have a combined thickness between 1 nanometer and 200 nanometers.

19. The device of any one of claims 1-18, wherein the active layer comprises at least one of an inorganic semiconductor material, an organic-inorganic semiconductor material, or an organic semiconductor material.

20. A method for reversibly switching a window integrated photovoltaic device between a first state and a second state, the method comprising:

a first reversible transferring of a molecule from a reservoir through at least a charge transport layer to an active layer;

intercalating the molecule in the active layer;

decalating the molecule from the active layer; and

a second reversible transferring of the molecule through at least the charge transport layer to the reservoir, wherein:

the first reversible transferring results in the first state,

while in the first state, the active layer is substantially transparent to visible light,

the second reversible transferring results in the second state,

while in the second state, the active layer is substantially opaque to visible light, and

while in the first state and the second state, the device is capable of converting at least a portion of light to electricity.

21. The method of claim 20, wherein:

the charge transport layer comprises a first layer and a second layer,

the first layer is in contact with the second layer,

the second layer is positioned between the first layer and the active layer,

the first layer comprises a first carbon nanostructure,

the second layer comprises a second carbon nanostructure, and

the charge transport layer is positioned between the active layer and the reservoir.

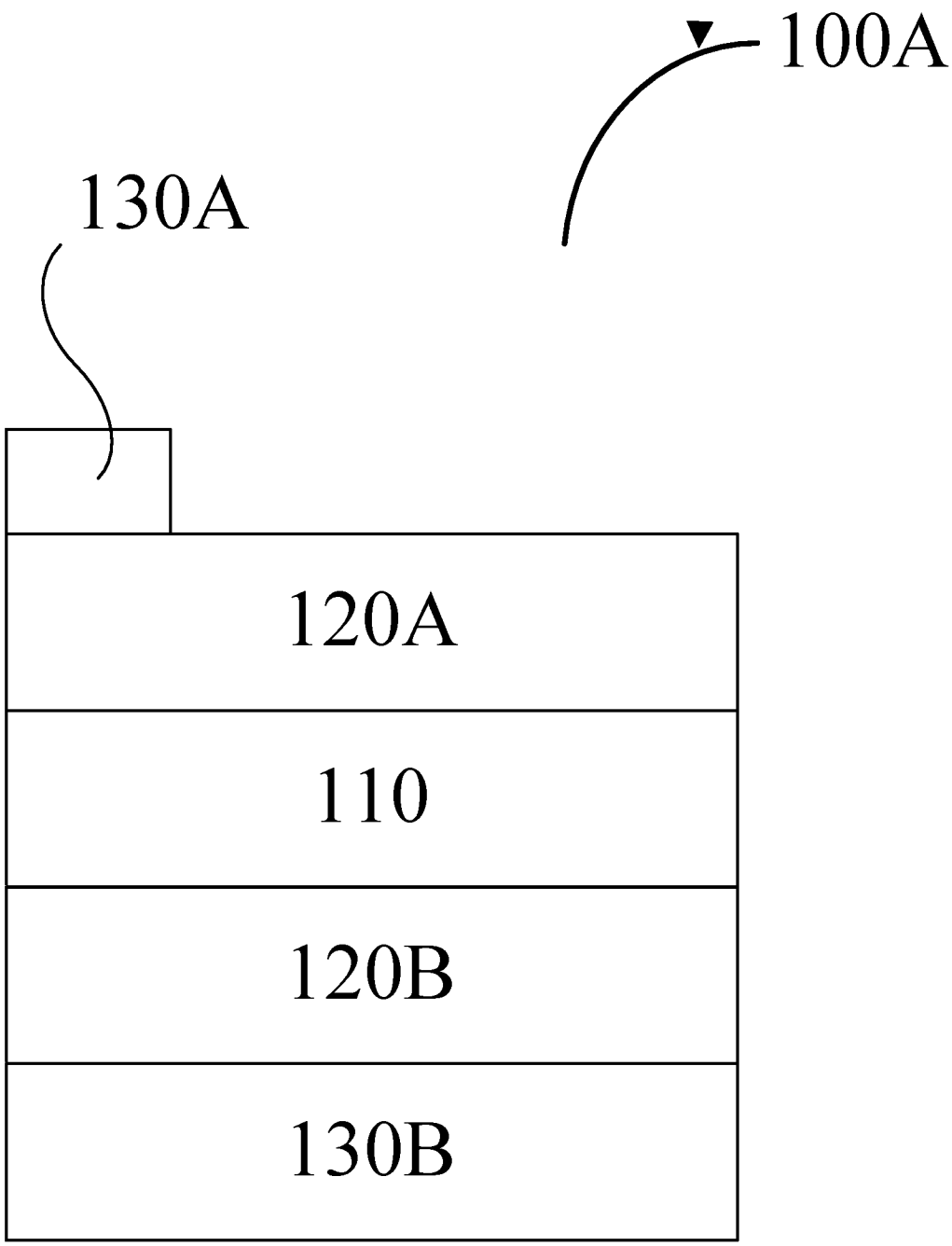

Figure 1

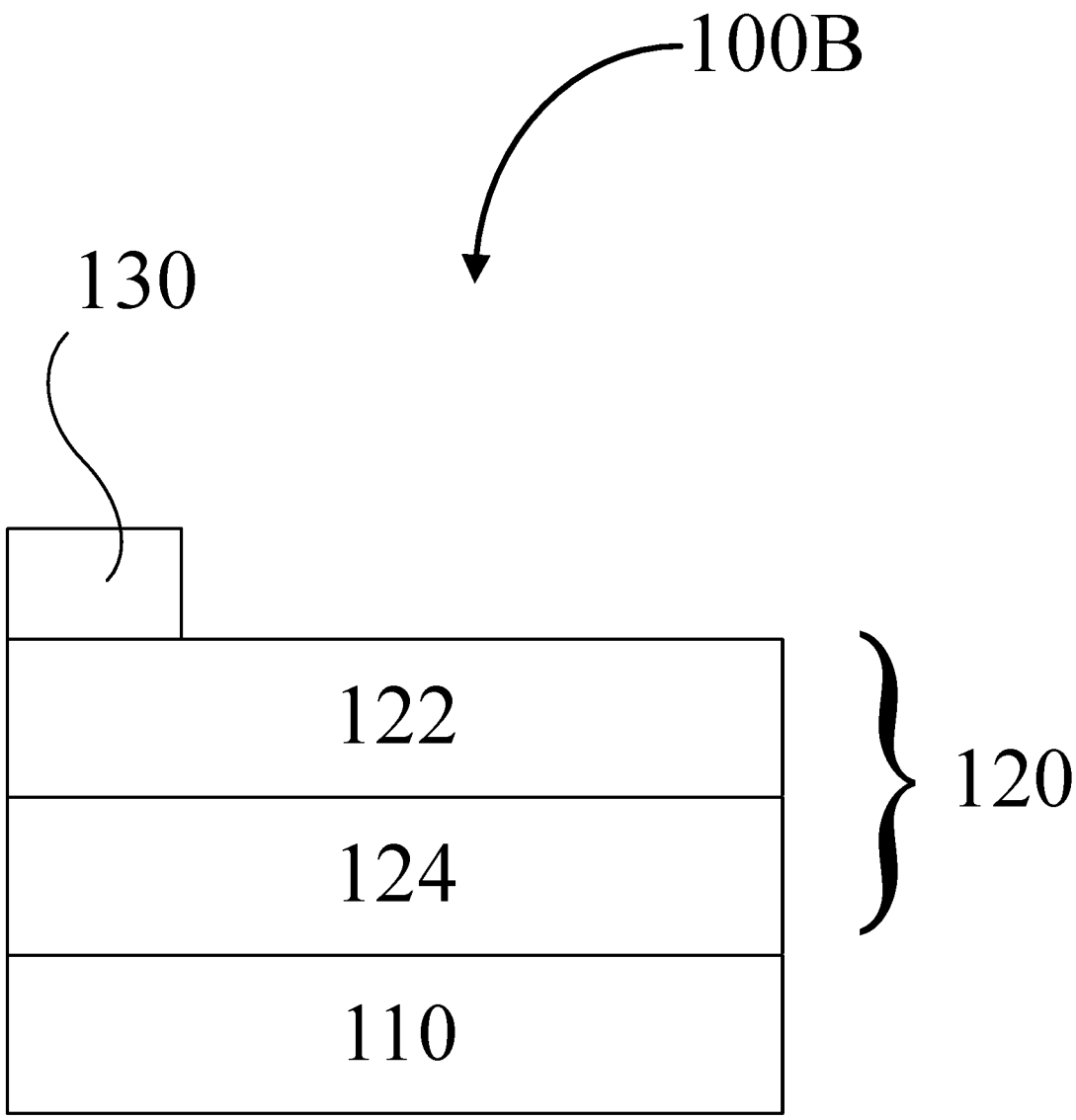

Figure 2

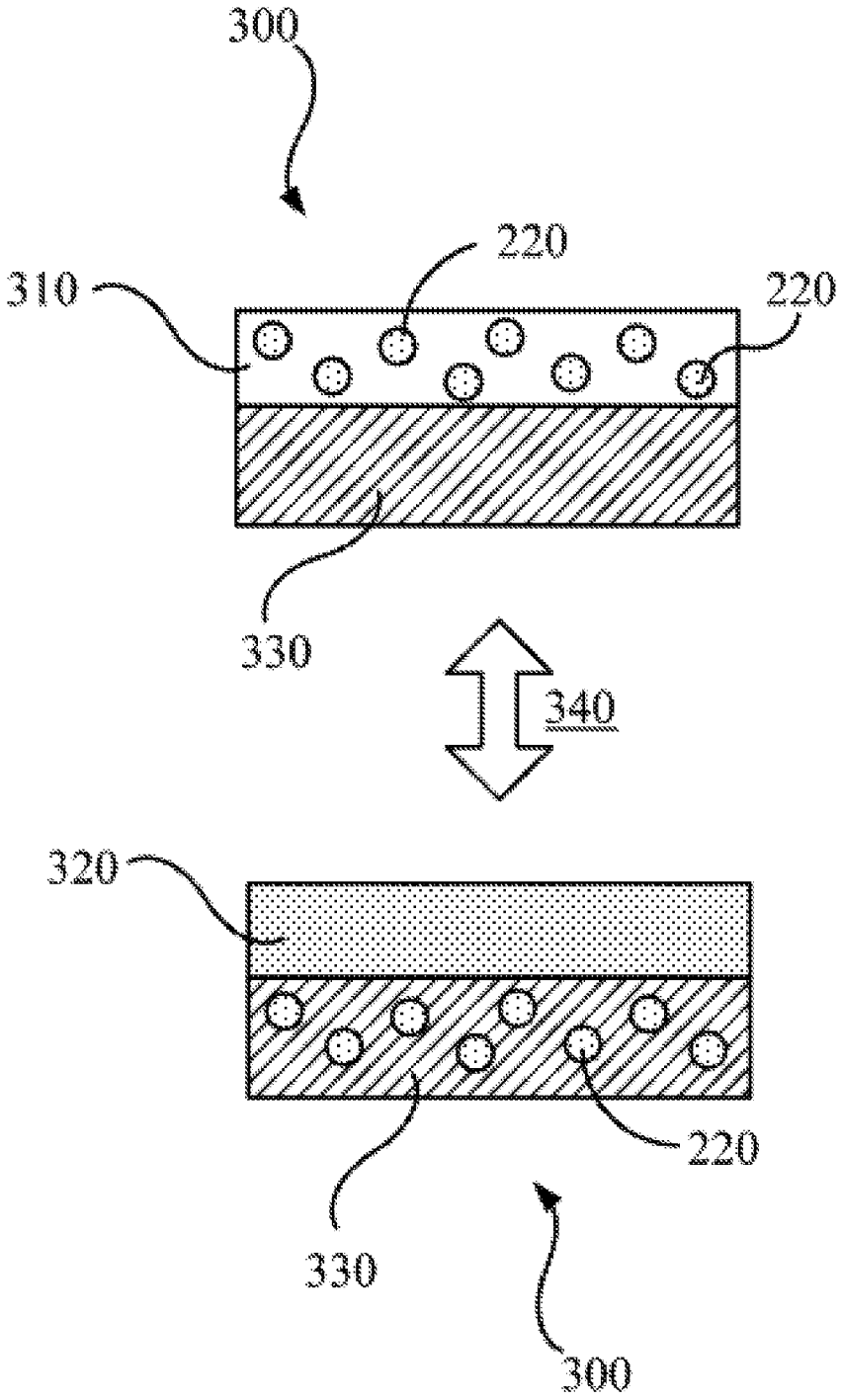

Figure 3

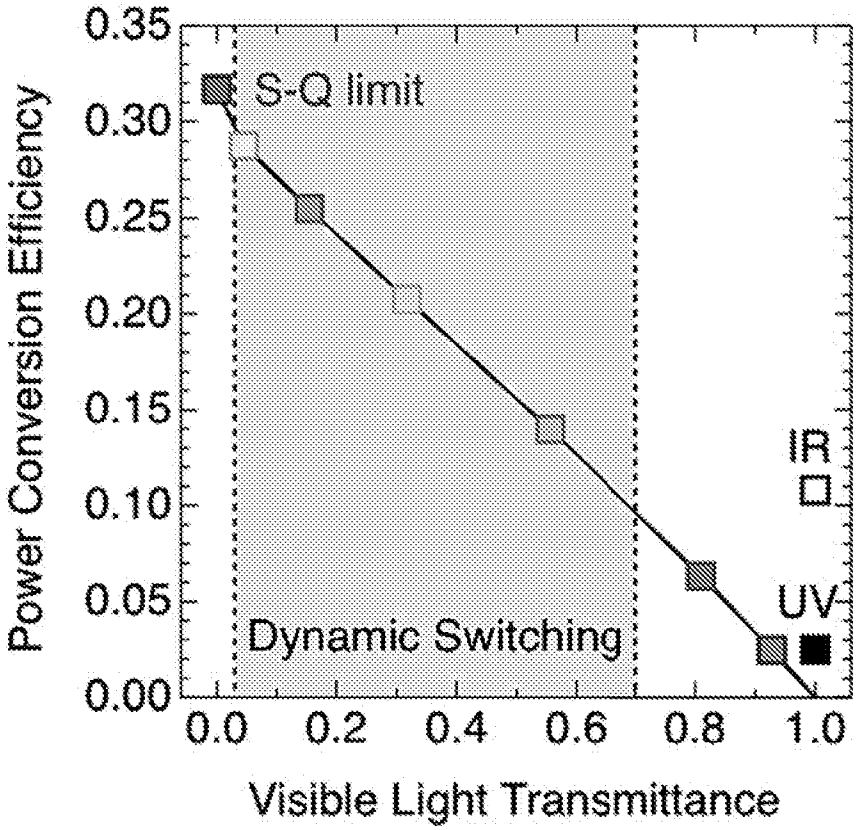
Power Conversion Efficiency
0.35
0.30
0.25
0.20
0.15
0.10
0.05
0.00
S-Q limit
Dynamic Switching
IR
UV
0.0
0.2
0.4
0.6
0.8
1.0
Visible Light Transmittance

Figure 4A

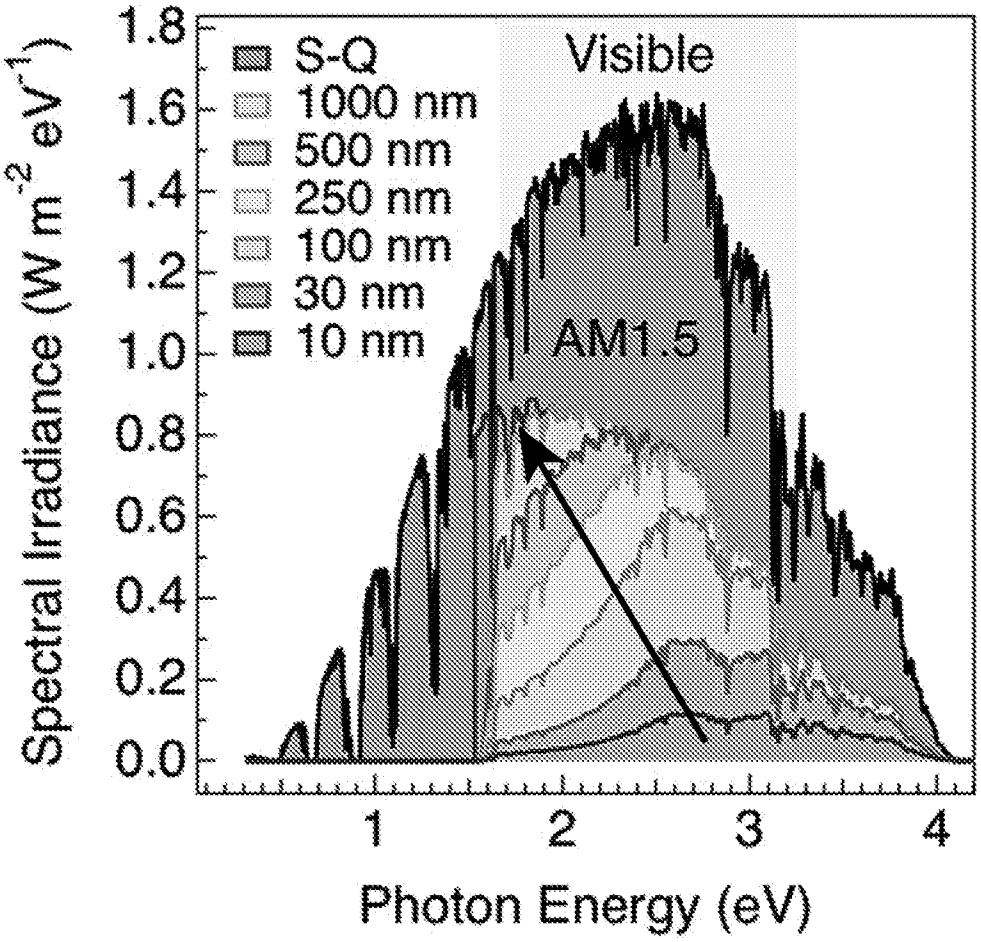
Spectral Irradiance (W m^{-2} eV^{-1})
1.8
1.6
1.4
1.2
1.0
0.8
0.6
0.4
0.2
0.0
S-Q
1000 nm
500 nm
250 nm
100 nm
30 nm
10 nm
Visible
AM1.5
1
2
3
4
Photon Energy (eV)

Figure 4B

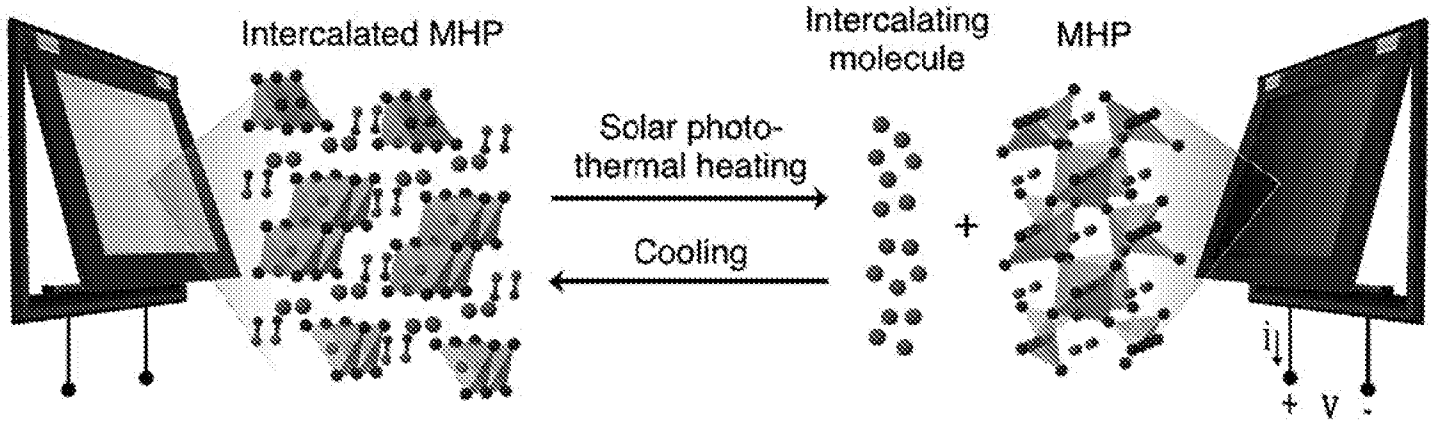
Intercalated MHP
Intercalating molecule
MHP
Solar photo-thermal heating
Cooling
+
i
+ V -

Figure 4C

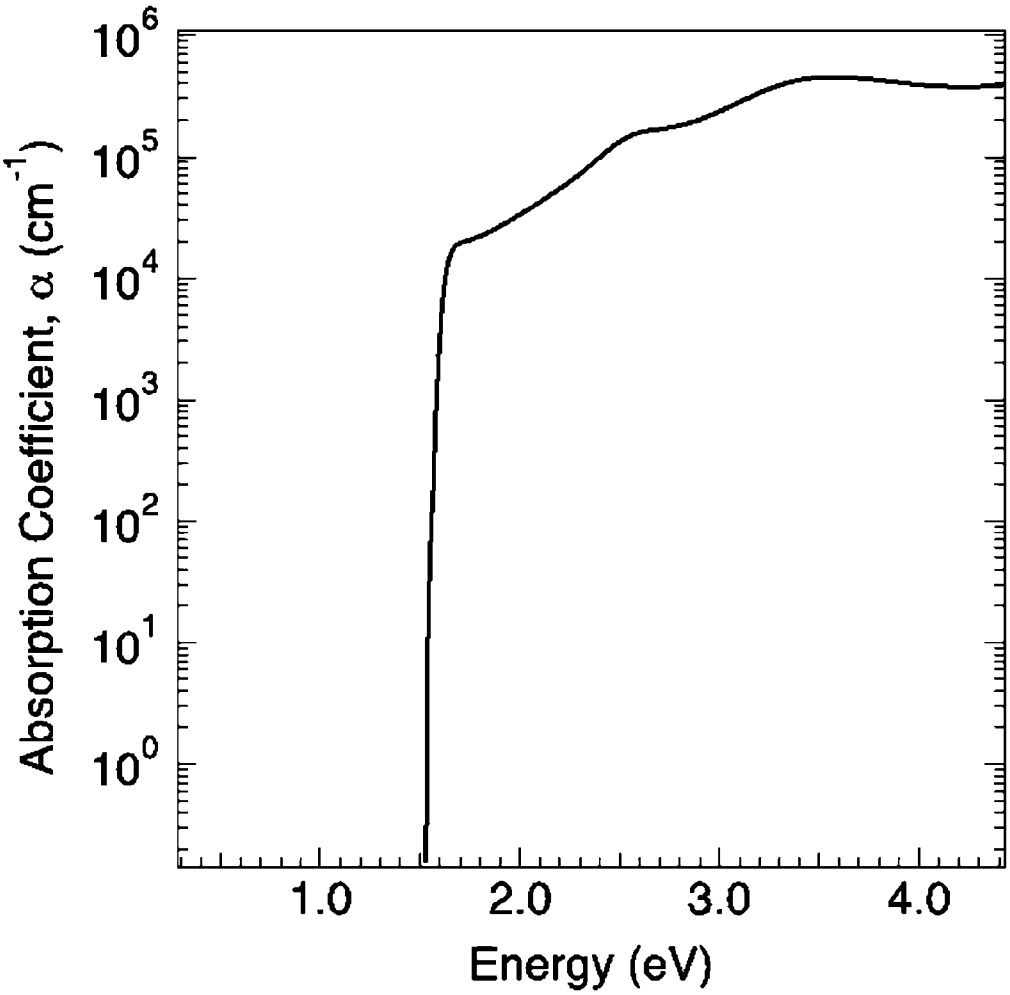
Absorption Coefficient, α (cm-1)
10^6
10^5
10^4
10^3
10^2
10^1
10^0
1.0
2.0
3.0
4.0
Energy (eV)

Figure 5

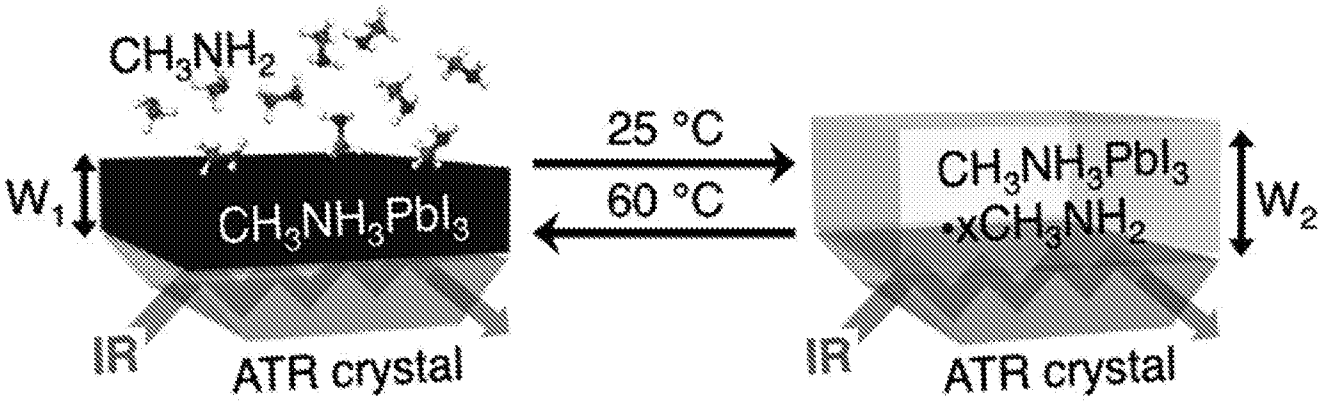
CH_3NH_2
W_1
$CH_3NH_3PbI_3$
IR
ATR crystal
25 °C
60 °C
$CH_3NH_3PbI_3$
$\bullet xCH_3NH_2$
W_2
IR
ATR crystal

Figure 6A

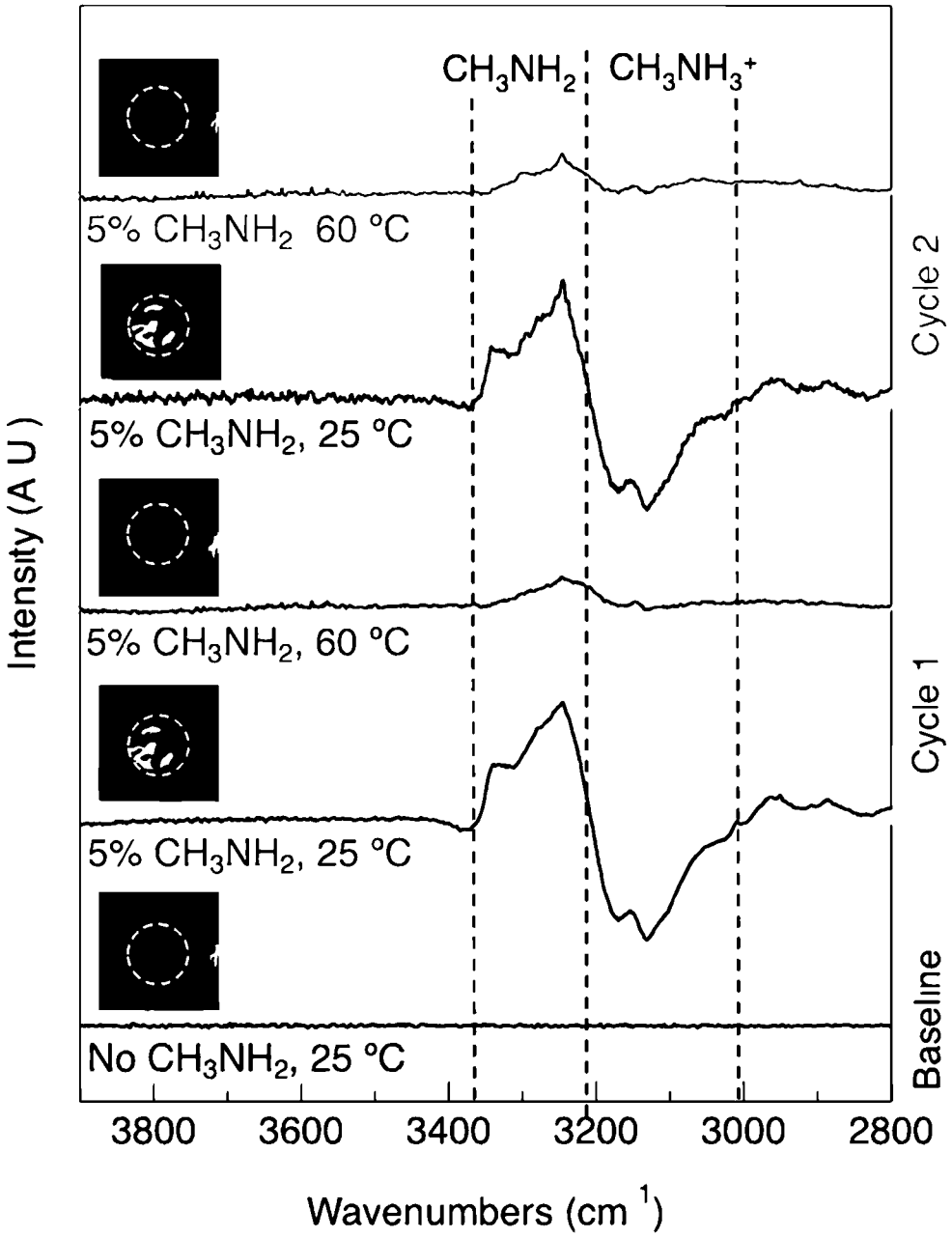
CH_3NH_2
$CH_3NH_3^+$
5% CH_3NH_2 60 °C
5% CH_3NH_2, 25 °C
5% CH_3NH_2, 60 °C
5% CH_3NH_2, 25 °C
No CH_3NH_2, 25 °C
Cycle 2
Cycle 1
Baseline
Intensity (A U)
3800
3600
3400
3200
3000
2800
Wavenumbers (cm^{-1})

Figure 6B

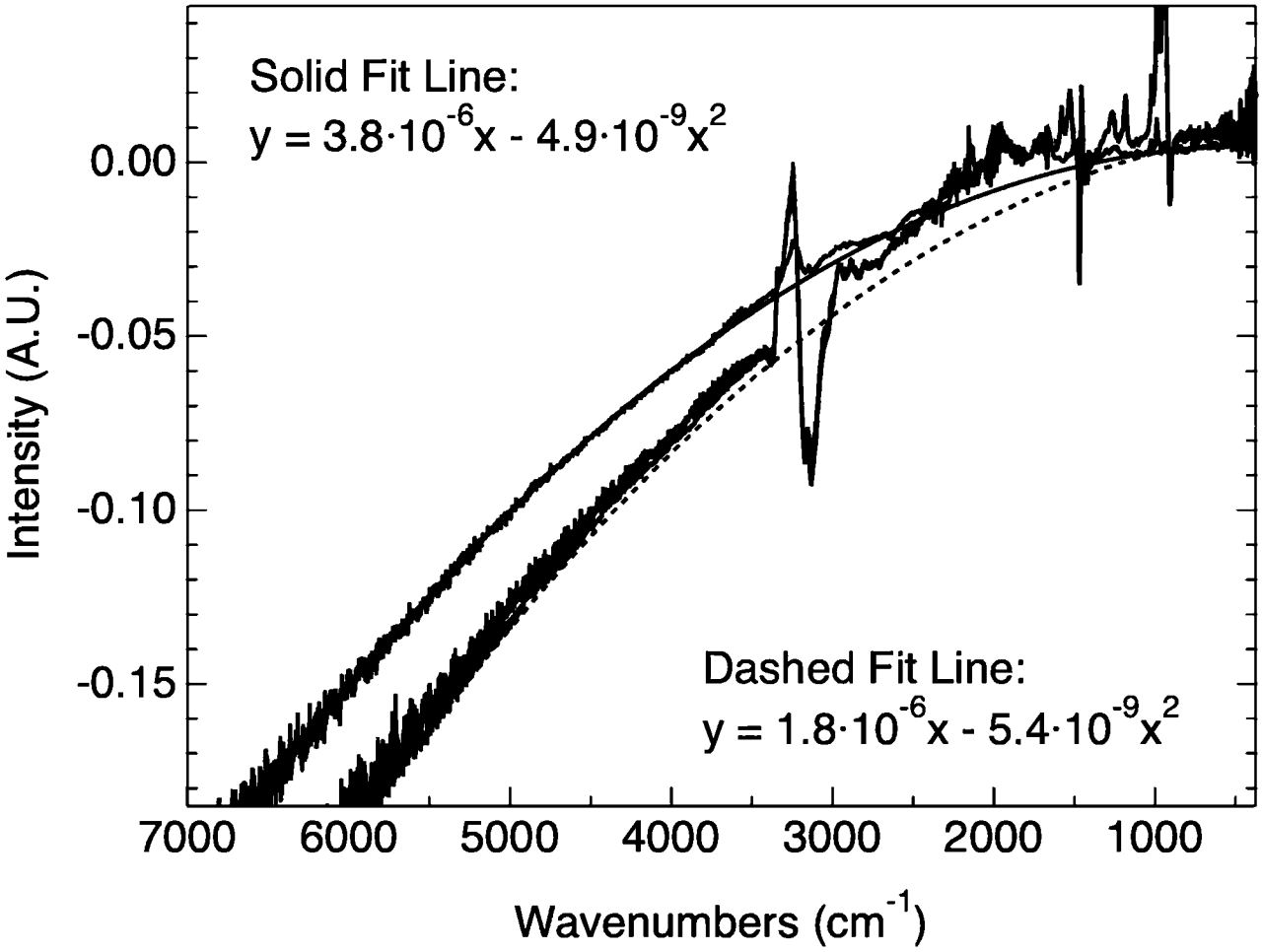
Solid Fit Line:
y = 3.8·10-6x - 4.9·10-9x2
Dashed Fit Line:
y = 1.8·10-6x - 5.4·10-9x2
Intensity (A.U.)
0.00
-0.05
-0.10
-0.15
7000
6000
5000
4000
3000
2000
1000
Wavenumbers (cm-1)

Figure 7

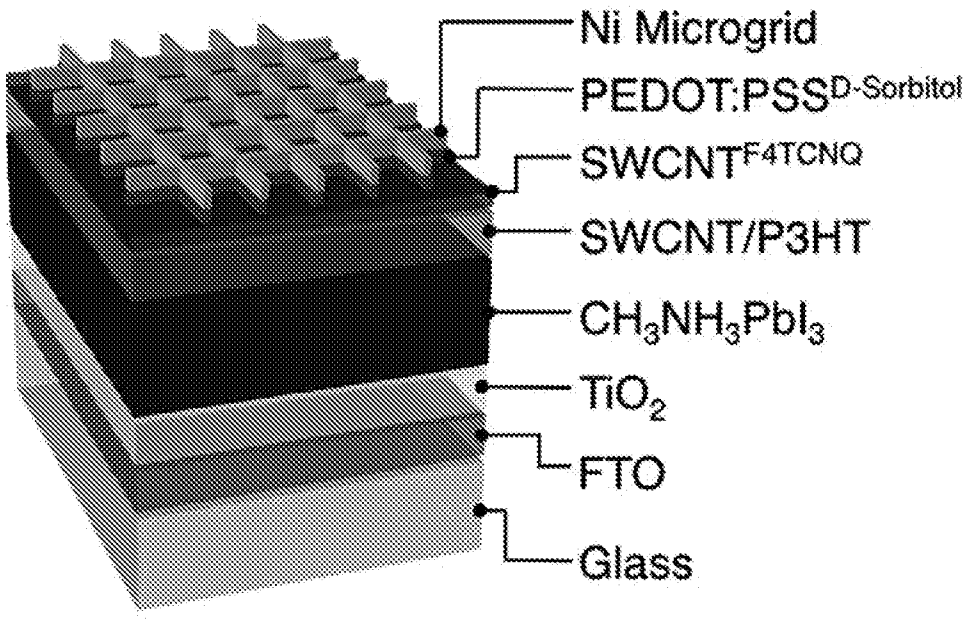
Ni Microgrid
PEDOT:PSS D-Sorbitol
SWCNT F4TCNQ
SWCNT/P3HT
$CH_3NH_3PbI_3$
TiO_2
FTO
Glass

Figure 8A

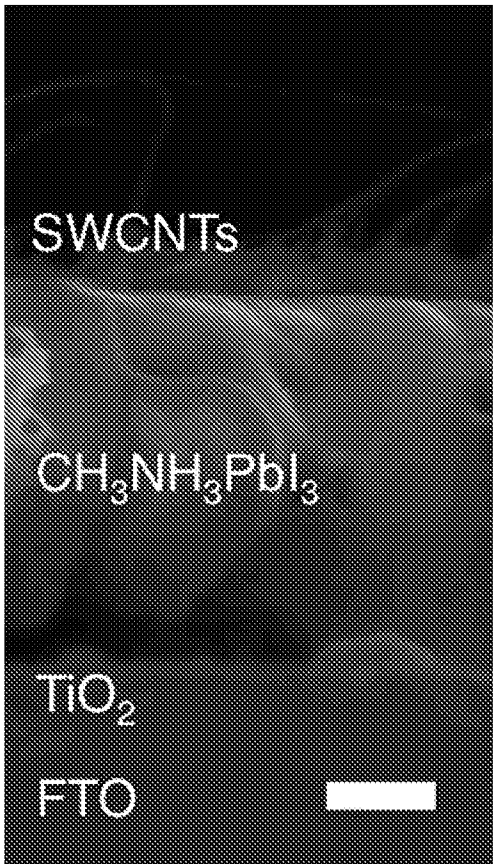

Figure 8B

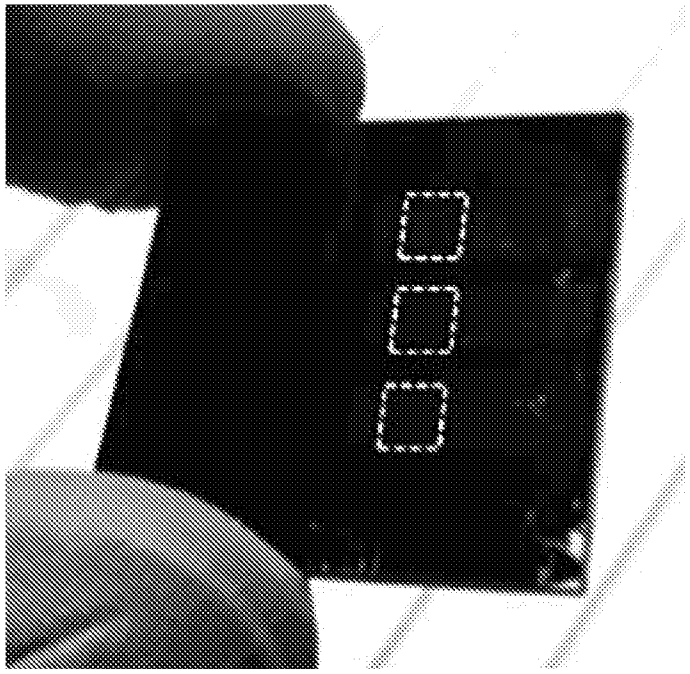

Figure 8C

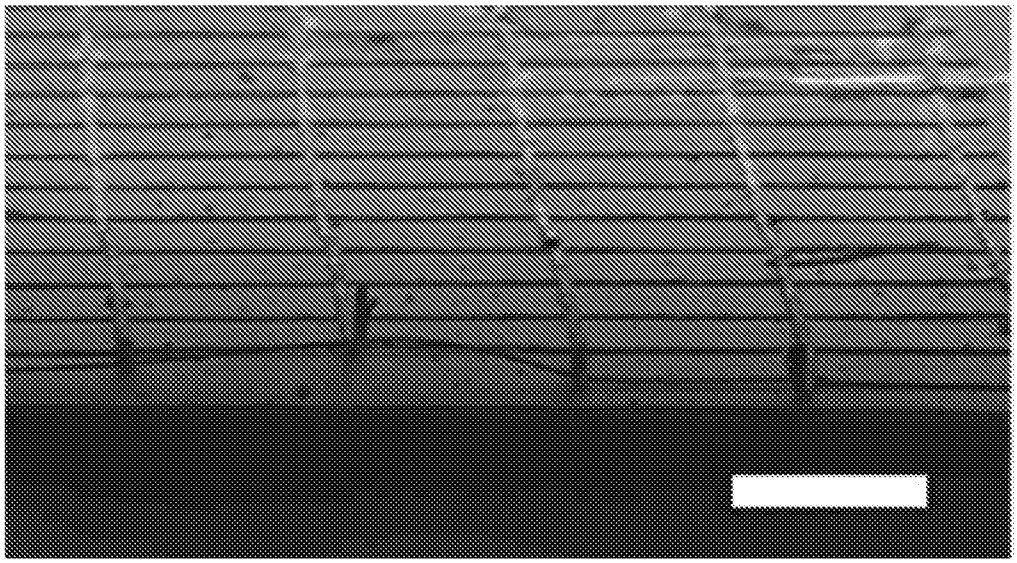

Figure 8D

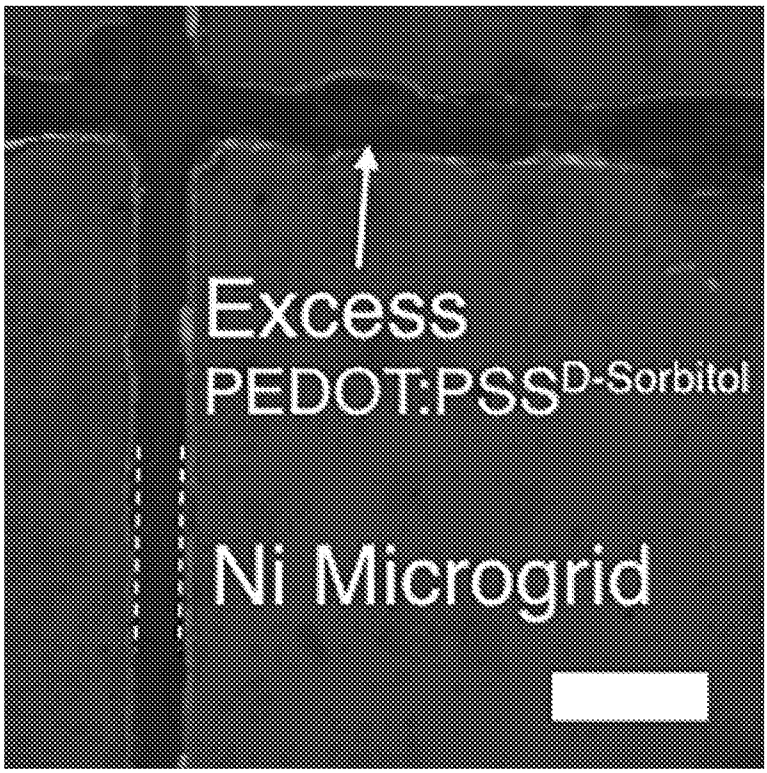

Figure 8E

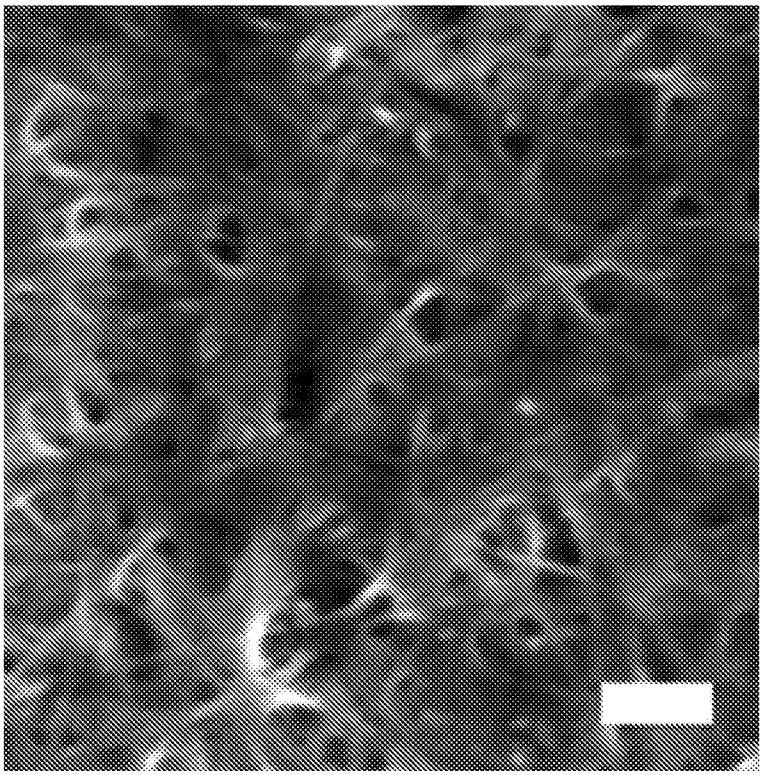

Figure 8F

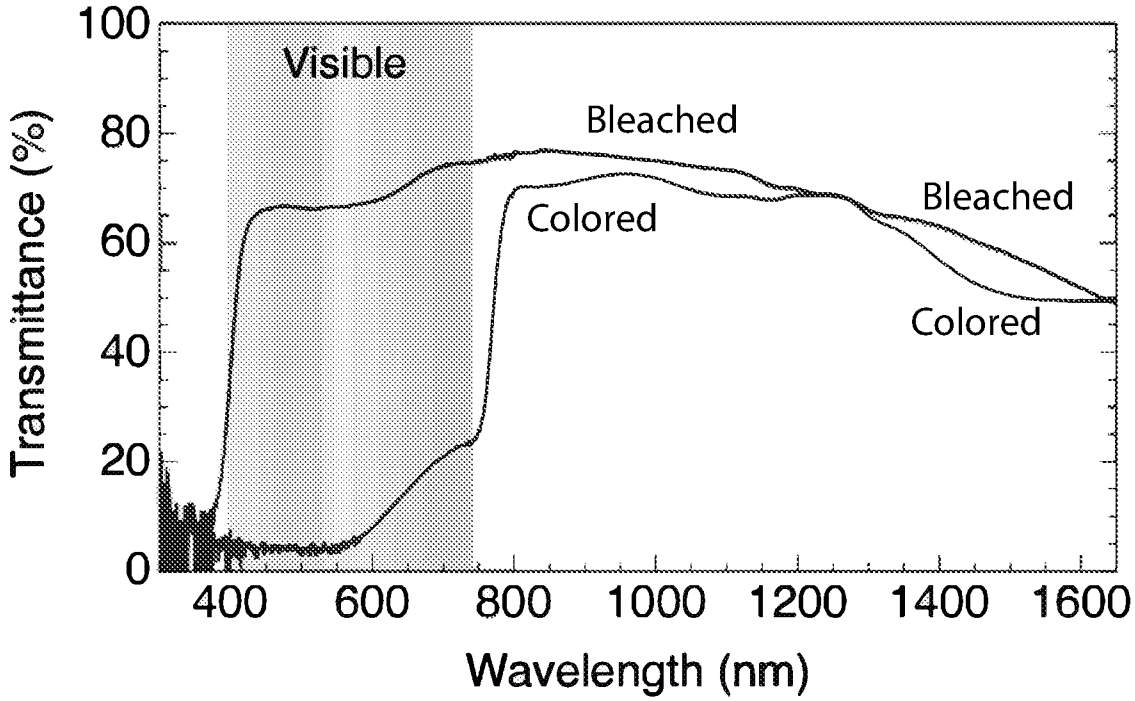
100
80
60
40
20
0
Transmittance (%)
Visible
Bleached
Colored
Bleached
Colored
400
600
800
1000
1200
1400
1600
Wavelength (nm)

Figure 8G

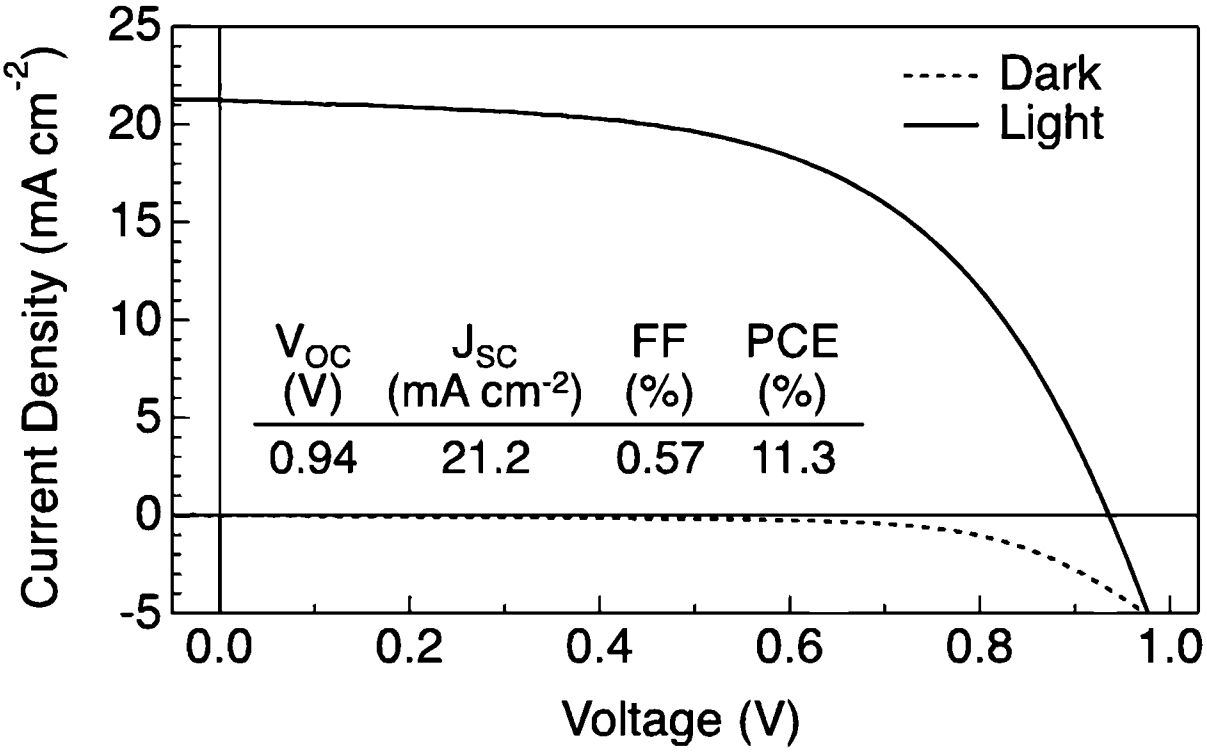
Current Density (mA cm-2)
25
20
15
10
5
0
-5
0.0
0.2
0.4
0.6
0.8
1.0
Voltage (V)
Dark
Light
VOC (V)
JSC (mA cm-2)
FF (%)
PCE (%)
0.94
21.2
0.57
11.3

Figure 8H

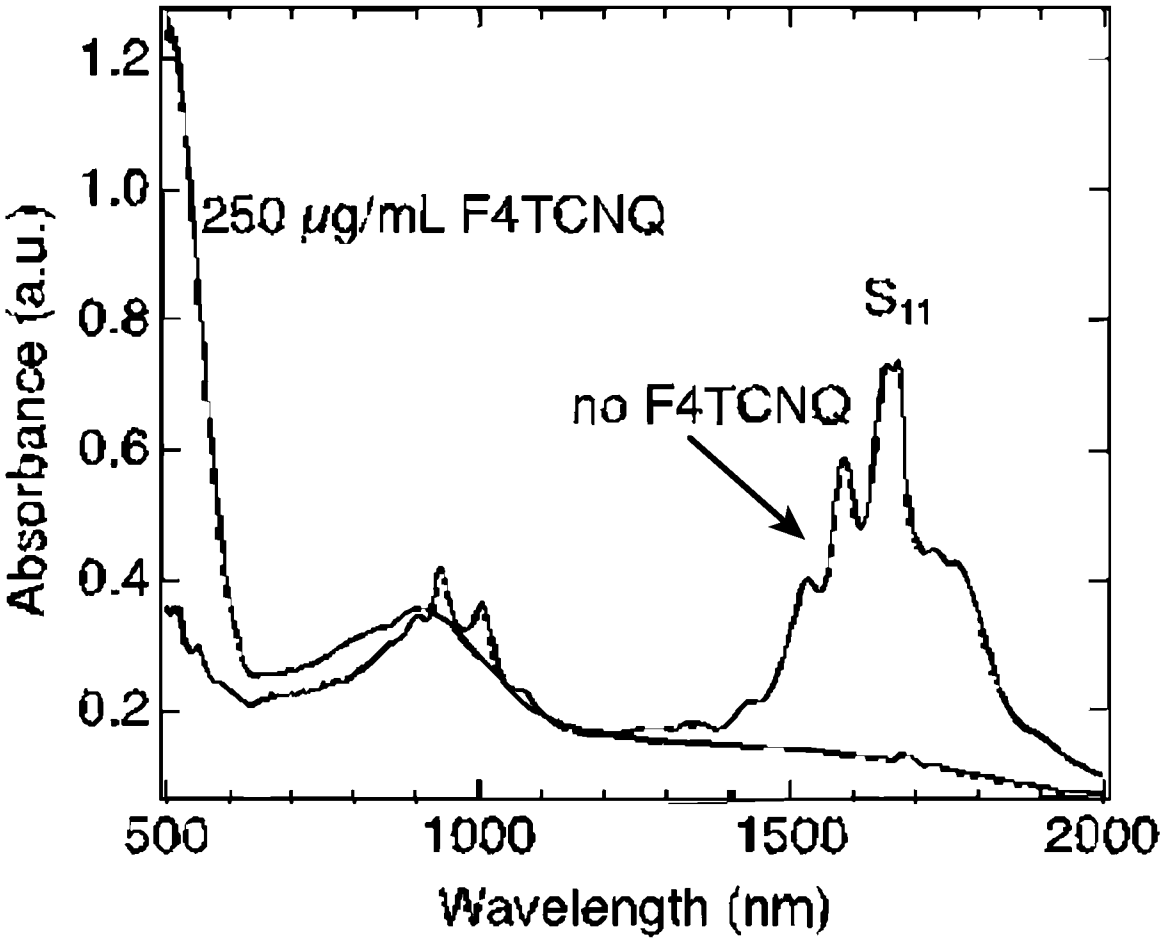
1.2
1.0
0.8
0.6
0.4
0.2
Absorbance (a.u.)
250 μg/mL F4TCNQ
S11
no F4TCNQ
500
1000
1500
2000
Wavelength (nm)

Figure 9

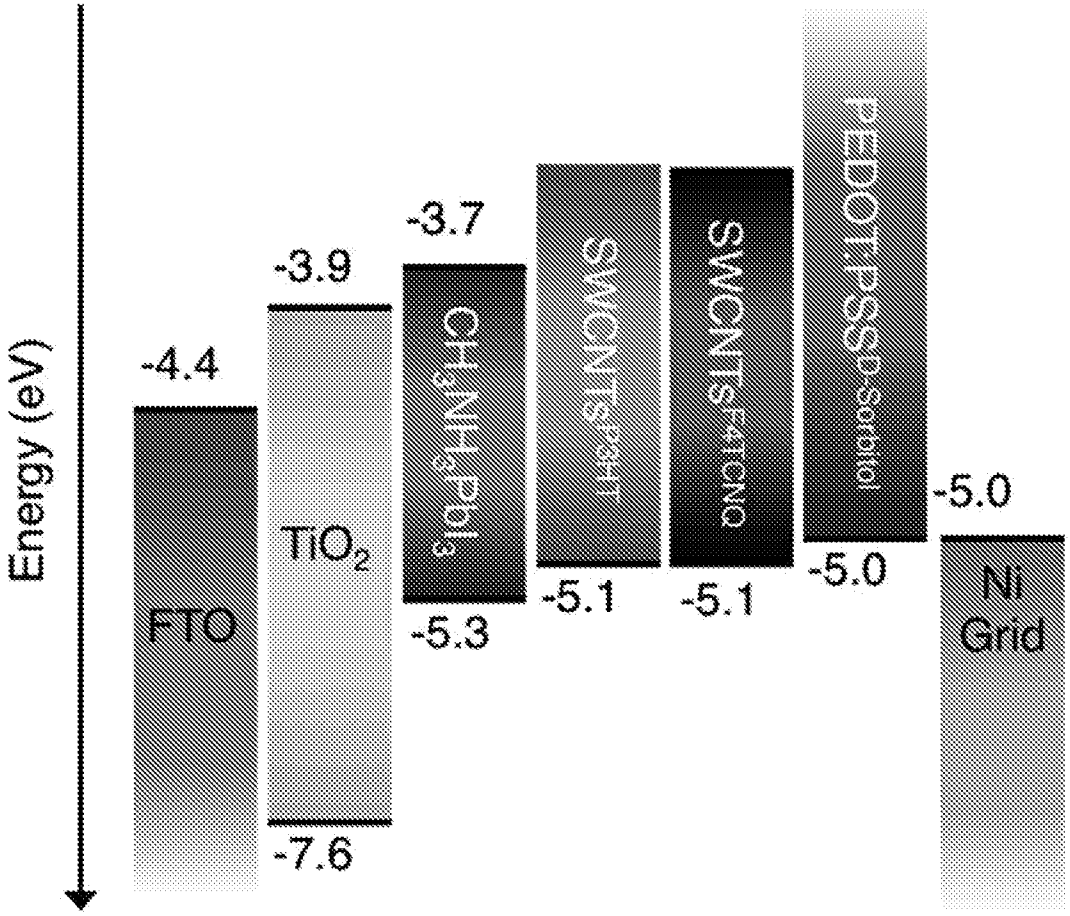
Energy (eV)
-4.4
FTO
-3.9
TiO2
-7.6
-3.7
CH3NH3PbI3
-5.3
SWCNTs-PCBM
-5.1
SWCNTs-TiCNO
-5.1
PEDOT:PSS-Surfactant
-5.0
-5.0
Ni Grid

Figure 10

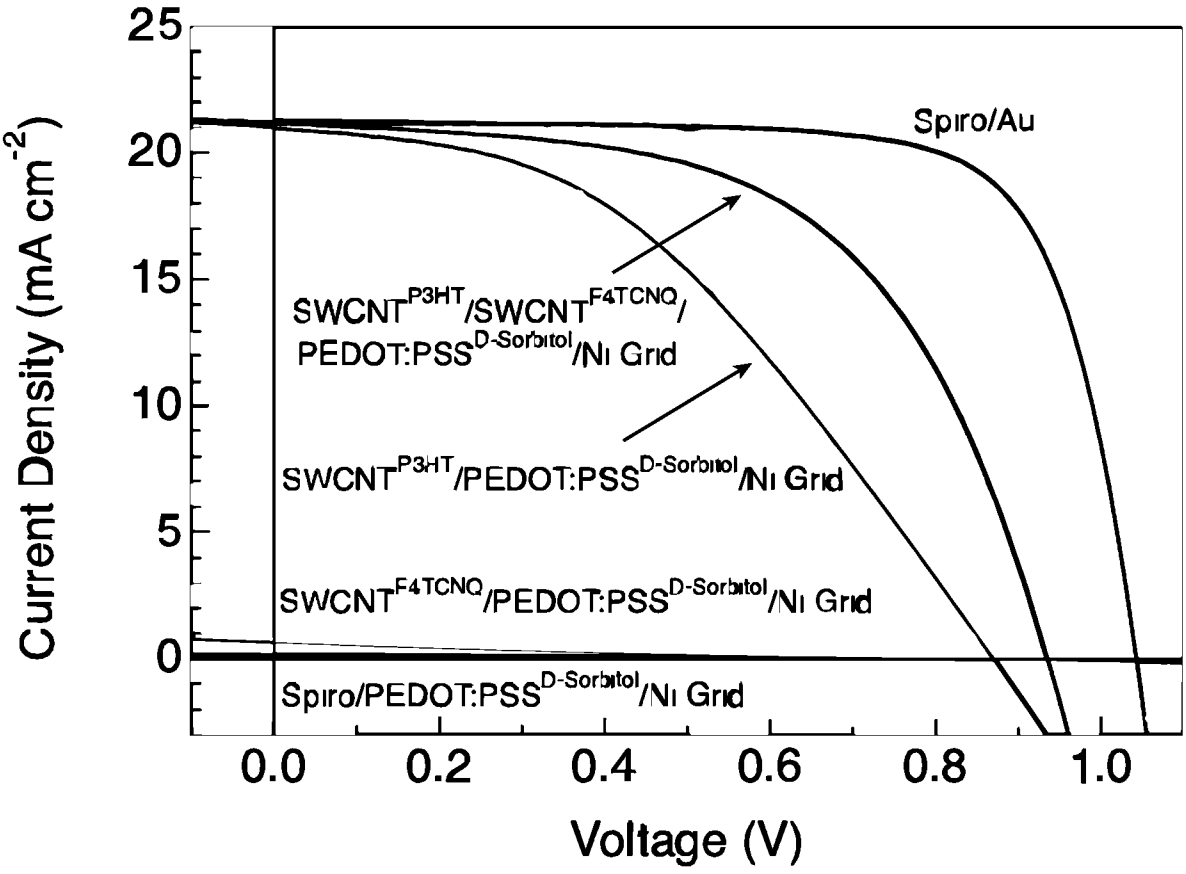
Current Density (mA cm-2)
25
20
15
10
5
0
0.0
0.2
0.4
0.6
0.8
1.0
Voltage (V)
Spiro/Au
SWCNTP3HT/SWCNTF4TCNQ/
PEDOT:PSSD-Sorbitol/Ni Grid
SWCNTP3HT/PEDOT:PSSD-Sorbitol/Ni Grid
SWCNTF4TCNQ/PEDOT:PSSD-Sorbitol/Ni Grid
Spiro/PEDOT:PSSD-Sorbitol/Ni Grid

Figure 11

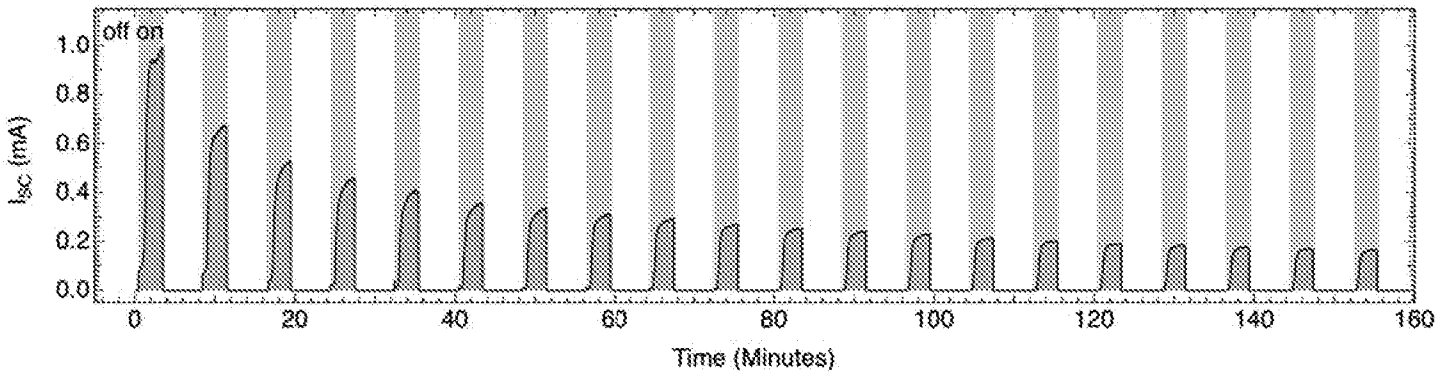
off on
1.0
0.8
0.6
0.4
0.2
0.0
I_{SC} (mA)
0
20
40
60
80
100
120
140
160
Time (Minutes)

Figure 12A

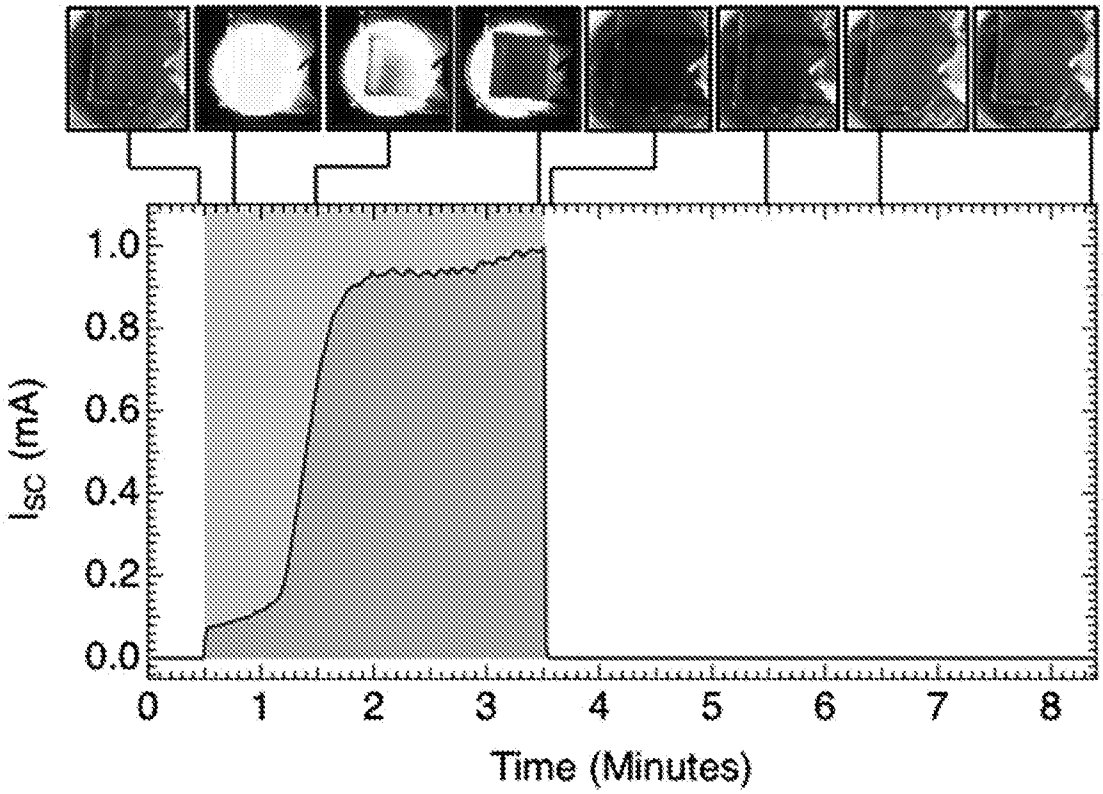

Figure 12B

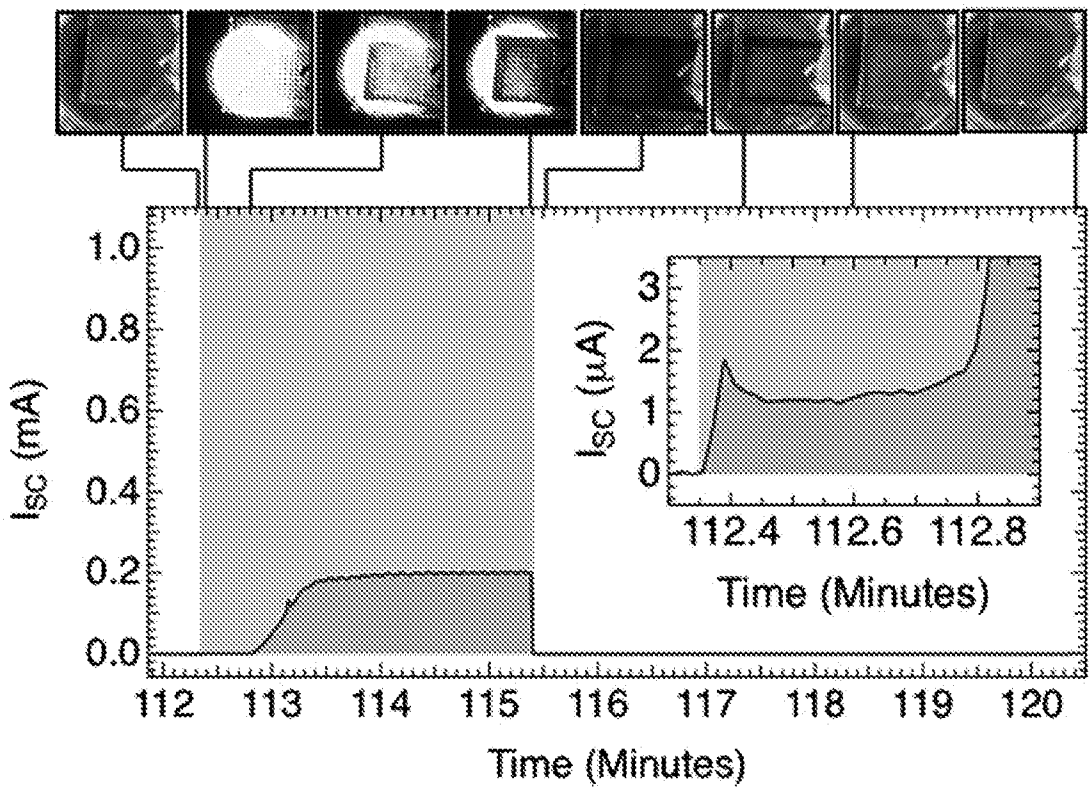
1.0
0.8
0.6
0.4
0.2
0.0
I_{SC} (mA)
112
113
114
115
116
117
118
119
120
Time (Minutes)
3
2
1
0
I_{SC} (μA)
112.4
112.6
112.8
Time (Minutes)

Figure 12C

INTERNATIONAL SEARCH REPORT

International application No.
PCT/US2018/032088

A. CLASSIFICATION OF SUBJECT MATTER

IPC(8) - G02F 1/01; E06B 9/24; H01L 51/44; H01L 51/46 (2018.01)
CPC - H01L 51/0048; H01L 51/42; E06B 9/24; G02F 1/0126 (2018.05)

According to International Patent Classification (IPC) or to both national classification and IPC

B. FIELDS SEARCHED

Minimum documentation searched (classification system followed by classification symbols)
See Search History document

Documentation searched other than minimum documentation to the extent that such documents are included in the fields searched

Electronic data base consulted during the international search (name of data base and, where practicable, search terms used)
See Search History document

C. DOCUMENTS CONSIDERED TO BE RELEVANT

Category*	Citation of document, with indication, where appropriate, of the relevant passages	Relevant to claim No.
X --- Y	US 2017/0089128 A1 (ALLIANCE FOR SUSTAINABLE ENERGY LLC) 30 March 2017 (30.03.2017) entire document	20 --- 1-3, 21
Y	NORTON-BAKER et al., Polymer-Free Carbon Nanotube Thermoelectrics with Improved Charge Carrier Transport and Power Factor, ACS Energy Letters, Vol. 1, 17 November 2016 [retrieved on 26 June 2018]. Retrieved from the internet: <URL: https://pubs.acs.org/doi/pdf/10.1021/acsenergylett.6b00417> Pgs. 1212-1220	1-3, 21
Y	US 2010/0132770 A1 (BEATTY et al) 03 June 2010 (03.06.2010) entire document	21

☐ Further documents are listed in the continuation of Box C. ☐ See patent family annex.

* Special categories of cited documents:

"A" document defining the general state of the art which is not considered to be of particular relevance

"E" earlier application or patent but published on or after the international filing date

"L" document which may throw doubts on priority claim(s) or which is cited to establish the publication date of another citation or other special reason (as specified)

"O" document referring to an oral disclosure, use, exhibition or other means

"P" document published prior to the international filing date but later than the priority date claimed

"T" later document published after the international filing date or priority date and not in conflict with the application but cited to understand the principle or theory underlying the invention

"X" document of particular relevance; the claimed invention cannot be considered novel or cannot be considered to involve an inventive step when the document is taken alone

"Y" document of particular relevance; the claimed invention cannot be considered to involve an inventive step when the document is combined with one or more other such documents, such combination being obvious to a person skilled in the art

"&" document member of the same patent family

Date of the actual completion of the international search	Date of mailing of the international search report
28 June 2018	12 JUL 2018
Name and mailing address of the ISA/US Mail Stop PCT, Attn: ISA/US, Commissioner for Patents P.O. Box 1450, Alexandria, VA 22313-1450 Facsimile No. 571-273-8300	Authorized officer Blaine R. Copenheaver PCT Helpdesk: 571-272-4300 PCT OSP: 571-272-7774

INTERNATIONAL SEARCH REPORT

International application No.
PCT/US2018/032088

Box No. II Observations where certain claims were found unsearchable (Continuation of item 2 of first sheet)

This international search report has not been established in respect of certain claims under Article 17(2)(a) for the following reasons:

1. ☐ Claims Nos.:
because they relate to subject matter not required to be searched by this Authority, namely:

2. ☐ Claims Nos.:
because they relate to parts of the international application that do not comply with the prescribed requirements to such an extent that no meaningful international search can be carried out, specifically:

3. ☒ Claims Nos.: 4-19
because they are dependent claims and are not drafted in accordance with the second and third sentences of Rule 6.4(a).

Box No. III Observations where unity of invention is lacking (Continuation of item 3 of first sheet)

This International Searching Authority found multiple inventions in this international application, as follows:

1. ☐ As all required additional search fees were timely paid by the applicant, this international search report covers all searchable claims.

2. ☐ As all searchable claims could be searched without effort justifying additional fees, this Authority did not invite payment of additional fees.

3. ☐ As only some of the required additional search fees were timely paid by the applicant, this international search report covers only those claims for which fees were paid, specifically claims Nos.:

4. ☐ No required additional search fees were timely paid by the applicant. Consequently, this international search report is restricted to the invention first mentioned in the claims; it is covered by claims Nos.:

Remark on Protest

☐ The additional search fees were accompanied by the applicant's protest and, where applicable, the payment of a protest fee.

☐ The additional search fees were accompanied by the applicant's protest but the applicable protest fee was not paid within the time limit specified in the invitation.

☐ No protest accompanied the payment of additional search fees.